Monthly Notices of the ROYAL ASTRONOMICAL SOCIETY

MNRAS **446,** 3034–3061 (2015) doi:10.1093/mnras/stu2260

The VMC Survey – XIII. Type II Cepheids in the Large Magellanic Cloud⋆

V. Ripepi,[1]† M. I. Moretti,[1,2,3] M. Marconi,[1] G. Clementini,[2] M.-R. L. Cioni,[4,5] R. de Grijs,[6,7] J. P. Emerson,[8] M. A. T. Groenewegen,[9] V. D. Ivanov,[10] T. Muraveva,[2] A. E. Piatti[11,12] and S. Subramanian[13]

[1]*INAF-Osservatorio Astronomico di Capodimonte, Via Moiariello 16, I-80131 Naples, Italy*
[2]*INAF-Osservatorio Astronomico di Bologna, via Ranzani 1, I-40127 Bologna, Italy*
[3]*Scuola Normale Superiore, Piazza dei Cavalieri, 7, I-56126 Pisa, Italy*
[4]*School of Physics, Astronomy and Mathematics, University of Hertfordshire, College Lane, Hatfield AL10 9AB, UK*
[5]*Leibnitz-Institut für Astrophysik Potsdam, An der Sternwarte 16, D-14482 Potsdam, Germany*
[6]*Kavli Institute for Astronomy and Astrophysics, Peking University, Yi He Yuan Lu 5, Hai Dian District, Beijing 100871, China*
[7]*Department of Astronomy, Peking University, Yi He Yuan Lu 5, Hai Dian District, Beijing 100871, China*
[8]*Astronomy Unit, School of Physics & Astronomy, Queen Mary University of London, Mile End Road, London E1 4NS, UK*
[9]*Koninklijke Sterrenwacht van België, Ringlaan 3, B-1180 Brussel, Belgium*
[10]*European Southern Observatory, Ave. Alonso de Cordova 3107, Casilla 19, Chile*
[11]*Observatorio Astronómico, Universidad Nacional de Córdoba, Laprida 854, 5000 Córdoba, Argentina*
[12]*Consejo Nacional de Investigaciones Científicas y Técnicas, Av. Rivadavia 1917, C1033AAJ, Buenos Aires, Argentina*
[13]*Indian Institute of Astrophysics, Koramangala, Bangalore 560 034, India*

Accepted 2014 October 27. Received 2014 October 25; in original form 2014 July 11

ABSTRACT

The VISTA (Visible and Infrared Survey Telescope for Astronomy) survey of the Magellanic Clouds System (VMC) is collecting deep K_s-band time-series photometry of the pulsating variable stars hosted in the system formed by the two Magellanic Clouds and the Bridge connecting them. In this paper, we have analysed a sample of 130 Large Magellanic Cloud (LMC) Type II Cepheids (T2CEPs) found in tiles with complete or near-complete VMC observations for which identification and optical magnitudes were obtained from the OGLE III (Optical Gravitational Lensing Experiment) survey. We present J and K_s light curves for all 130 pulsators, including 41 BL Her, 62 W Vir (12 pW Vir) and 27 RV Tau variables. We complement our near-infrared photometry with the V magnitudes from the OGLE III survey, allowing us to build a variety of period–luminosity (PL), period–luminosity–colour (PLC) and period–Wesenheit (PW) relationships, including any combination of the V, J, K_s filters and valid for BL Her and W Vir classes. These relationships were calibrated in terms of the LMC distance modulus, while an independent absolute calibration of the PL(K_s) and the PW(K_s, V) was derived on the basis of distances obtained from *Hubble Space Telescope* parallaxes and Baade–Wesselink technique. When applied to the LMC and to the Galactic globular clusters hosting T2CEPs, these relations seem to show that (1) the two Population II standard candles RR Lyrae and T2CEPs give results in excellent agreement with each other; (2) there is a discrepancy of ∼0.1 mag between Population II standard candles and classical Cepheids when the distances are gauged in a similar way for all the quoted pulsators. However, given the uncertainties, this discrepancy is within the formal 1σ uncertainties.

Key words: surveys – stars: oscillations – stars: Population II – stars: variables: Cepheids – galaxies: distances and redshifts – Magellanic Clouds.

1 INTRODUCTION

The Magellanic Clouds (MCs) are fundamental benchmarks in the framework of stellar populations and galactic evolution investigations (see e.g. Harris & Zaritsky 2004, 2009; Ripepi et al. 2014b).

⋆Based on observations made with VISTA at ESO under programme ID 179.B-2003.

†E-mail: ripepi@oacn.inaf.it

The ongoing interaction with the Milky Way also allows us to study in detail the complex mechanisms that rule the interaction among galaxies (see e.g. Putman et al. 1998; Muller et al. 2004; Stanimirović, Staveley-Smith & Jones 2004; Bekki & Chiba 2007; Venzmer, Kerp & Kalberla 2012; For, Staveley-Smith & McClure-Griffiths 2013). Additionally, the MCs are more metal poor than our Galaxy and host a large population of young populous clusters; thus, they are useful to test the physical and numerical assumptions at the basis of stellar evolution codes (see e.g. Matteucci et al. 2002; Brocato et al. 2004; Neilson & Langer 2012).

The Large Magellanic Cloud (LMC) is also fundamental in the context of the extragalactic distance scale. Indeed, it represents the first critical step on which the calibration of classical Cepheid (CC) period–luminosity (PL) relations and in turn of secondary distance indicators relies (see e.g. Freedman et al. 2001; Riess et al. 2011; Walker 2012, and references therein). At the same time, the LMC hosts several thousand of RR Lyrae variables, which represent the most important Population II standard candles through the well-known M_V(RR)–[Fe/H] and near-infrared (NIR) metal-dependent PL relations. Moreover, the LMC contains tens of thousands of intermediate-age red clump stars, which can profitably be used as accurate distance indicators (see e.g. Laney, Joner & Pietrzyński 2012; Subramanian & Subramaniam 2013). Hence, the LMC is the ideal place to compare the distance scales derived from Population I and II indicators (see e.g. Clementini et al. 2003; Walker 2012; de Grijs, Wicker & Bono 2014, and references therein). In particular, NIR observations of pulsating stars (see e.g. Ripepi et al. 2012a, 2014a; Moretti et al. 2014, and references therein) provide stringent constraints to the calibration of their distance scale thanks to the existence of well-defined PL, period–luminosity–colour (PLC) and period–Wesenheit (PW) relations at these wavelengths (see Madore 1982; Madore & Freedman 1991, for the definition of Wesenheit functions).

The VISTA[1] near-infrared YJK_s survey of the Magellanic Clouds system (VMC; Cioni et al. 2011) aims at observing a wide area across the Magellanic system, including the relatively unexplored Bridge connecting the two Clouds. This European Southern Observatory (ESO) public survey relies on the VISTA InfraRed CAMera (VIRCAM) (Dalton et al. 2006) of the ESO VISTA telescope (Emerson, McPherson & Sutherland 2006) to obtain deep NIR photometric data in the Y, J and K_s filters. The main aims are (i) to reconstruct the spatially resolved star formation history and (ii) to infer an accurate 3D map of the whole Magellanic system. The properties of pulsating stars observed by VMC and adopted as tracers of three different stellar populations, namely CCs (younger than few hundred Myr), RR Lyrae stars (older than 9–10 Gyr) and anomalous Cepheids (traditionally associated with an intermediate-age population with few Gyr), have been discussed in recent papers by our team (Ripepi et al. 2012a,b, 2014a; Moretti et al. 2014). In these papers, relevant results on the calibration of the distance scales for all these important standard candles have been provided.

An additional class of Population II pulsating stars is represented by the so-called Type II Cepheids (T2CEPs; see e.g. Caputo 1998; Sandage & Tammann 2006). These objects show periods from ∼1 to ∼20 d and are observed in Galactic globular clusters (GGCs) with few RR Lyrae stars and blue horizontal branch morphology. They are brighter but less massive than RR Lyrae stars for similar metal content (see e.g. Caputo et al. 2004). T2CEPs are often separated into BL Herculis stars (BL Her; periods between 1 and 4 d) and W Virginis stars (W Vir; periods between 4 and 20 d) and, as discussed by several authors (e.g. Wallerstein & Cox 1984; Gingold 1985; Harris 1985; Bono, Caputo & Santolamazza 1997b; Wallerstein 2002), originate from hot, low-mass stellar structures, starting their central He burning on the blue side of the RR Lyrae gap. Moreover, according to several authors (see e.g. Feast et al. 2008; Feast 2010, and references therein) RV Tauri stars, with periods from about 20 to 150 d and often irregular light curves, are considered as an additional subgroup of the T2CEP class. Their evolutionary phase corresponds to the post-asymptotic giant branch phase path towards planetary nebula status. This feature corresponds to the latest evolution of intermediate mass stellar structures and for this reason the claimed link with the low-mass W Vir stars should be considered with caution.

In addition to the three quoted groups, Soszyński et al. (2008) suggested the existence of a new sub-class of T2CEPs, the so-called peculiar W Vir (pW Vir) stars. These objects show peculiar light curves and, at constant period, are usually brighter than normal T2CEPs. It is likely that pW Vir belong to binary systems; however, the true nature of these variables remains uncertain.

Nemec, Nemec & Lutz (1994) derived metal-dependent PL relations in various optical photometric bands both in the fundamental and in the first overtone modes but subsequently Kubiak & Udalski (2003) found that all the observed T2CEPs in the OGLE II (Optical Gravitational Lensing Experiment; Udalski et al. 1992) sample, with periods in the range ∼0.7 to about 10 d, satisfy the same PL relation. This result was then confirmed by Pritzl et al. (2003) and Matsunaga et al. (2006) for GGCs, by Groenewegen, Udalski & Bono (2008) for the Galactic bulge and again by Soszyński et al. (2008) on the basis of OGLE III data.

From the theoretical point of view, Di Criscienzo et al. (2007) and Marconi & Di Criscienzo (2007) have investigated the properties of BL Her stars, by adopting an updated evolutionary and pulsational scenario for metallicities in the range of $Z = 0.0001$–0.004. The predicted PL and PW relations derived on the basis of these models were found to be in good agreement with the slopes determined by the variables observed in GGCs. Moreover, the distances obtained from the theoretical relations for T2CEPs agree within the errors with the RR Lyrae-based values.

In the NIR bands, a tight PL for 46 T2CEPs hosted in GGCs was found by Matsunaga et al. (2006). Such relations were calibrated by Feast et al. (2008) by means of pulsation parallaxes of nearby T2CEPs and used to estimate the distances of the LMC and the Galactic Centre. Subsequent investigations (Matsunaga, Feast & Menzies 2009; Matsunaga, Feast & Soszyński 2011) confirmed the existence of such tight PL relations in the J, H, K_s bands for the T2CEPs belonging to the LMC and Small Magellanic Cloud found by the OGLE III collaboration (Soszyński et al. 2008). However, the NIR observations at the base of these studies consist of only two epochs for each variable light curve obtained with the Infrared Survey Facility (IRSF) 1.4 m telescope in South Africa. The average magnitudes of the T2CEPs analysed in that paper were derived by comparison with the OGLE III I-band photometry.

In the context of the VMC survey, we present here the NIR results for a significant sample of T2CEPs in the LMC, based on high precision and well-sampled K_s-band light curves.

The VMC data for the T2CEPs are presented in Section 2. The PL, PLC and PW relations involving the J and K_s bands are calculated in Section 3. Section 4 includes the absolute calibration of such relations and a comparison with the literature. In Sections 5, we discuss the results; a concise summary (Section 6) concludes the paper.

[1] Visible and Infrared Survey Telescope for Astronomy.

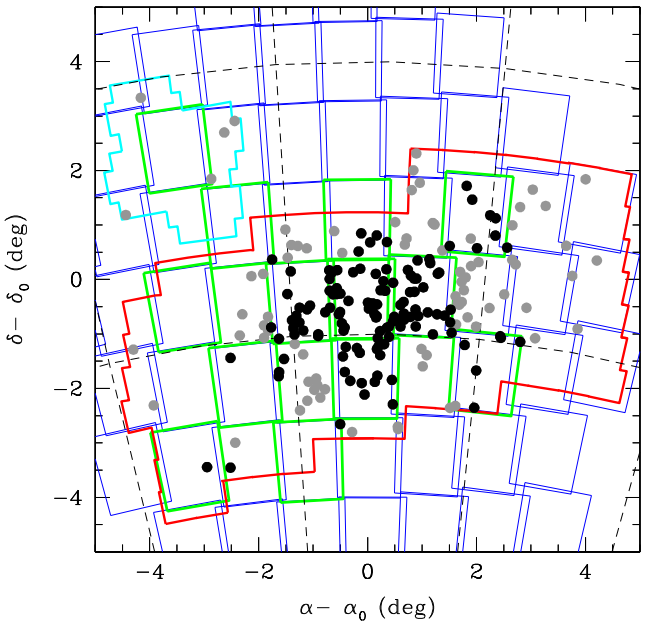

Figure 1. Distribution of the known T2CEPs over the LMC (projected on the sky adopting $\alpha_0 = 81.0$ deg and $\delta_0 = -69.0$ deg). Grey symbols show all the T2CEPs detected by the OGLE collaboration, whereas black filled circles present the T2CEPs falling in the VMC tiles and studied in this paper. Thin blue and thick green squares (distorted by the projection into the sky) show part of the VMC tiles in the LMC and the 13 tiles treated in this paper, respectively. The thick red and light blue lines show the areas covered by OGLE III and IV (released to date), respectively.

2 T2CEPS IN THE VMC SURVEY

T2CEPs in the LMC were identified and studied in the *V*, *I* optical bands by Soszyński et al. (2008) in the context of the OGLE III project.[2] We have also considered the recent early release of the OGLE IV survey (Soszyński et al. 2012), including the South Ecliptic Pole which, in turn, lies within our tile LMC 8_8. In these surveys, a total of 207 T2CEPs were found (203 by OGLE III and 4 by OGLE IV[3]), of which 65 are BL Her, 98 are W Vir and 44 are RV Tau pulsators.

In this paper, we present results for the T2CEPs included on 13 'tiles' (1.5 deg^2) completely or nearly completely observed, processed and catalogued by the VMC survey as of 2013 March (and overlapping with the area investigated by OGLE III), namely the tiles LMC 4_6, 4_8, 5_3, 5_5, 5_7, 6_4, 6_5, 6_6, 6_8, 7_3, 7_5, 7_7 and 8_8 (see Fig. 1 and Table 1). Tile LMC 6_6 is centred on the well-known 30 Dor star-forming region; tiles LMC 5_5, 6_4 and 6_5 are placed on the bar of the LMC. The remaining tiles lie in less crowded regions of the galaxy.

A detailed description of the general observing strategy of the VMC survey can be found in Cioni et al. (2011). As for the variable stars, the specific procedures adopted to study these objects were discussed in Moretti et al. (2014). Here, we only briefly recall that the VMC K_s-band time-series observations were scheduled in 12 separate epochs distributed over several consecutive months. This strategy allows us to obtain well-sampled light curves for a variety of variable types (including RR Lyrae variables and Cepheids of all types). Concerning the *J* and *Y* bands, the average number of epochs is 3, as a result of the observing strategy in these bands (i.e. monitoring was not planned). Hence, some epochs could occur in the same night and even one after the other. We note that in this paper, we did not consider the *Y*-band data for several reasons: (i) this filter is very rarely used in the context of distance scale; (ii) its photometric zero-point (ZP) is difficult to calibrate (no 2MASS measures); (iii) because the *Y* band is bluer than the typical NIR bands, and the PL, PLC and PW relations in this filter are expected to be more dispersed (see e.g. Madore & Freedman 2012) and of lesser utility with respect to those in *J* and K_s.

Table 1. Number of T2CEPs in the 13 VMC tiles analysed in this paper, according to OGLE III/IV.

Tile LMC	RA (centre) J(2000)	Dec. (centre) J(2000)	n_{T2CEP}
LMC 4_6	05:38:00.41	−72:17:20.0	1
LMC 4_8	06:06:32.95	−72:08:31.2	2
LMC 5_3	04:58:11.66	−70:35:28.0	6
LMC 5_5	05:24:30.34	−70:48:34.2	17
LMC 5_7	05:51:04.87	−70:47:31.2	4
LMC 6_4	05:12:55.80	−69:16:39.4	33
LMC 6_5	05:25:16.27	−69:21:08.3	31
LMC 6_6	05:37:40.01	−69:22:18.1	20
LMC 6_8	06:02:22.00	−69:14:42.4	0
LMC 7_3	05:02:55.20	−67:42:14.8	9
LMC 7_5	05:25:58.44	−67:53:42.0	6
LMC 7_7	05:49:12.19	−67:52:45.5	1
LMC 8_8	05:59:23.14	−66:20:28.7	0

The VMC data, processed through the pipeline (Irwin et al. 2004) of the VISTA Data Flow System (VDFS; Emerson et al. 2004) are in the VISTA photometric system (Vegamag = 0). The time-series photometry used in this paper was retrieved from the VISTA Science Archive[4] (VSA; Cross et al. 2012). For details about the data reduction, we refer the reader to the aforementioned papers. Nevertheless, we underline two characteristics of the data reduction which we think may have importance in the subsequent discussion. First, the pipeline is able to correct the photometry of stars close to the saturation limit (Irwin 2009). This is relevant in the context of this paper because the RV Tau variables discussed here are very bright objects $K_s \sim 12$–13 mag, close to the saturation limits of the VMC survey. The photometry of these stars takes advantage of the VDFS ability to treat saturated images; however, as we will see below, the corrections applied are not always sufficient to fully recover the data. Secondly, the data retrieved from VSA include quality flags which are very useful to understand if the images have problems. We shall use this information later in this paper.

According to OGLE III/IV, 130 T2CEPs are expected to lie in the 13 tiles analysed in this paper. Note that no T2CEP from OGLE III or OGLE IV falls inside our tiles 6_8 or 8_8, respectively. Hence, in the following we only use OGLE III data. Fig. 1 and Table 1 show the distribution of such stars through the VMC tiles.

Table 2 lists the 130 T2CEPs analysed here, together with their main properties as measured by OGLE III and the information about the VMC tile they belong to, as well as the number of epochs of observations in the *J* and K_s bands. In total, our sample is composed of 41 BL Her, 62 W Vir (12 pW Vir) and 27 RV Tau variables, corresponding to 63, 63 (75 per cent) and 61 per cent of the

[2] Data available at http://ogle.astrouw.edu.pl

[3] Soszyński et al. (2012) also report the discovery of one yellow semiregular variable (SRd). Since this class of variables is not considered in this paper, we ignore this object in the present work.

[4] http://horus.roe.ac.uk/vsa/

Table 2. Cross-identification and main characteristics of the T2CEPs in the 13 'tiles' analysed in this paper. The columns report (1) OGLE identification; (2) right ascension (OGLE); (3) declination (OGLE); (4) variability class; (5) intensity-averaged I magnitude (OGLE); (6) intensity-averaged V magnitude (OGLE); (7) period (OGLE); (8) epoch of maximum light −2450 000 d (OGLE); (9) VMC identification as in the internal VSA release VMC v1.2/v1.3(2013 August 5); (10) VMC tile; (11) number of J and K_s epochs, respectively; (12) notes on individual stars.

ID	RA J2000	Dec. J2000	Type	$\langle I \rangle$ (mag)	$\langle V \rangle$ (mag)	Period (d)	Epoch (d)	VMC-ID	Tile	$N_{\rm Epochs}$ J,K_s	Notes
(1)	(2)	(3)	(4)	(5)	(6)	(7)	(8)	(9)	(10)	(11)	(12)
OGLE-LMC-T2CEP-123	5:26:19.26	−70:15:34.7	BL Her	18.233	18.723	1.002 626	454.802 33	558361325273	5_5	4,15	(a); (b)
OGLE-LMC-T2CEP-069	5:14:56.77	−69:40:22.4	BL Her	18.372	18.919	1.021 254	457.218 15	558355522273	6_4	4,14	(a); (b); (c)
OGLE-LMC-T2CEP-114	5:23:29.75	−68:19:07.2	BL Her	18.068	19.020	1.091 089	2167.449 39	558353567228	7_5	4,14	(b)
OGLE-LMC-T2CEP-020	4:59:06.12	−67:45:24.6	BL Her	18.036	18.469	1.108 126	2166.108 54	558351437065	7_3	4,16	(a); (b)
OGLE-LMC-T2CEP-071	5:15:08.63	−68:54:53.5	BL Her	17.872	18.382	1.152 164	457.433 79	558354926512	6_4	4,14	
OGLE-LMC-T2CEP-089	5:18:35.72	−69:45:45.7	BL Her	18.032	18.492	1.167 298	455.651 66	558355569068	6_4	11,23	
OGLE-LMC-T2CEP-061	5:12:30.42	−69:07:16.2	BL Her	18.018	18.588	1.181 512	457.305 01	558355098130	6_4	4,14	
OGLE-LMC-T2CEP-107	5:22:05.79	−69:40:24.5	BL Her	17.684	18.482	1.209 145	455.573 77	558356704139	6_5	7,9	(d); (e)
OGLE-LMC-T2CEP-077	5:16:21.44	−69:36:59.2	BL Her	17.762	18.039	1.213 802	456.996 03	558355472930	6_4	4,14	
OGLE-LMC-T2CEP-165	5:38:15.29	−69:28:57.1	BL Her	18.761	19.723	1.240 833	2187.683 39	558357659836	6_6	5,14	
OGLE-LMC-T2CEP-102	5:21:19.67	−69:56:56.2	BL Her	17.758	18.231	1.266 018	455.072 85	558356982625	6_5	7,9	(d); (e)
OGLE-LMC-T2CEP-194	5:57:12.03	−72:17:13.3	BL Her	17.874	18.447	1.314 467	2194.110 08	558367367174	4_8	5,10	
OGLE-LMC-T2CEP-136	5:29:48.11	−69:35:32.1	BL Her	17.823	18.095	1.323 038	454.373 19	558356602471	6_5	7,9	(b)
OGLE-LMC-T2CEP-138	5:30:10.87	−68:49:17.1	BL Her	18.059	18.827	1.393 591	2167.524 91	558356009909	6_5	7,9	(b); (d)
OGLE-LMC-T2CEP-109	5:22:12.83	−69:41:50.6	BL Her	19.559	21.212	1.414 553	454.695 80	558356727002	6_5	7,9	(c); (d)
OGLE-LMC-T2CEP-105	5:21:58.32	−70:16:35.1	BL Her	17.645	18.206	1.489 298	830.773 86	558361351217	5_5	4,15	
OGLE-LMC-T2CEP-122	5:25:48.19	−68:29:11.4	BL Her	18.241	19.028	1.538 669	2167.450 87	558353653819	7_5	4,14	
OGLE-LMC-T2CEP-171	5:39:40.96	−69:58:01.3	BL Her	17.824	18.512	1.554 749	726.828 05	558358012379	6_6	5,14	
OGLE-LMC-T2CEP-068	5:14:27.05	−68:58:02.0	BL Her	17.671	18.264	1.609 301	456.512 94	558354968904	6_4	4,14	
OGLE-LMC-T2CEP-124	5:26:55.80	−68:51:53.9	BL Her	17.889	18.614	1.734 867	2167.638 18	558356040530	6_5	7,9	
OGLE-LMC-T2CEP-008	4:51:11.51	−69:57:27.0	BL Her	17.842	18.585	1.746 099	2165.203 69	558358656758	5_3	4,11	(c); (d); (f)
OGLE-LMC-T2CEP-142	5:30:34.92	−68:06:15.2	BL Her	17.580	18.458	1.760 753	2167.011 20	558353450542	7_5	4,13	(a); (b); (g)
OGLE-LMC-T2CEP-084	5:17:07.50	−69:27:34.1	BL Her	17.512	17.841	1.770 840	456.088 00	558355348031	6_4	1,8	(a); (b); (g)
OGLE-LMC-T2CEP-141	5:30:23.32	−71:39:00.6	BL Her	17.975	18.757	1.822 954	2166.564 37	558367767291	4_6	6,14	
OGLE-LMC-T2CEP-140	5:30:22.71	−69:15:38.6	BL Her	17.760	18.508	1.841 144	2166.657 00	558356311759	6_5	7,9	
OGLE-LMC-T2CEP-144	5:31:19.82	−68:51:54.9	BL Her	17.750	18.545	1.937 450	2166.593 87	558356035425	6_5	10,20	(a); (b); (d); (f)
OGLE-LMC-T2CEP-130	5:29:04.24	−70:41:37.9	BL Her	17.527	18.124	1.944 694	2167.584 69	558361658078	5_5	4,15	
OGLE-LMC-T2CEP-088	5:18:33.57	−70:50:19.2	BL Her	17.212	17.353	1.950 749	2161.242 95	558361779217	5_5	4,15	(c); (d); (e)
OGLE-LMC-T2CEP-116	5:23:55.90	−69:25:30.1	BL Her	17.825	18.658	1.966 679	445.612 78	558356464708	6_5	7,9	
OGLE-LMC-T2CEP-121	5:25:42.79	−70:20:46.1	BL Her	17.713	18.430	2.061 365	2166.374 79	558361402653	5_5	4,15	
OGLE-LMC-T2CEP-166	5:38:29.09	−69:45:06.3	BL Her	16.927	17.696	2.110 599	2186.166 94	558357846207	6_6	5,14	(h)
OGLE-LMC-T2CEP-064	5:13:55.87	−68:37:52.1	BL Her	17.514	18.151	2.127 891	2167.008 43	558354745198	6_4	4,14	
OGLE-LMC-T2CEP-167	5:39:02.56	−69:37:38.5	BL Her	17.781	18.597	2.311 824	2187.148 39	558357756388	6_6	5,14	
OGLE-LMC-T2CEP-092	5:19:23.63	−70:02:56.8	BL Her	17.401	18.143	2.616 768	2122.719 33	558357072491	6_5	8,24	
OGLE-LMC-T2CEP-148	5:31:52.26	−69:30:26.4	BL Her	17.442	18.194	2.671 734	453.911 38	558357678615	6_6	12,23	
OGLE-LMC-T2CEP-195	6:02:46.27	−72:12:47.0	BL Her	17.342	18.050	2.752 929	2186.990 00	558367354217	4_8	5,10	
OGLE-LMC-T2CEP-113	5:23:06.33	−69:32:20.5	BL Her	17.137	17.811	3.085 460	455.010 03	558356568619	6_5	7,9	(b); (e)
OGLE-LMC-T2CEP-049	5:09:21.88	−69:36:03.0	BL Her	17.130	17.703	3.235 275	723.912 43	558355501190	6_4	4,14	(b)
OGLE-LMC-T2CEP-145	5:31:46.42	−68:58:44.0	BL Her	16.726	17.209	3.337 302	2167.280 23	558357363019	6_6	12,23	
OGLE-LMC-T2CEP-085	5:18:12.87	−71:17:15.4	BL Her	17.142	17.888	3.405 095	2160.554 57	558362047285	5_5	4,15	
OGLE-LMC-T2CEP-030	5:03:35.82	−68:10:16.2	BL Her	16.948	17.755	3.935 369	2166.206 73	558351663560	7_3	4,16	(a); (b); (g)
OGLE-LMC-T2CEP-134	5:29:28.49	−69:48:00.4	pW Vir	16.268	16.851	4.075 726	454.540 80	558356809300	6_5	7,9	
OGLE-LMC-T2CEP-173	5:39:49.93	−69:50:52.9	W Vir	18.416	20.149	4.147 881	724.817 27	558357918488	6_6	5,14	(a); (b)
OGLE-LMC-T2CEP-120	5:25:29.55	−68:48:11.8	W Vir	17.002	17.880	4.559 053	2165.735 88	558356005996	6_5	7,9	
OGLE-LMC-T2CEP-052	5:09:59.34	−69:58:28.7	pW Vir	16.395	16.861	4.687 925	2164.810 82	558355737497	6_4	4,14	
OGLE-LMC-T2CEP-098	5:20:25.00	−70:11:08.7	pW Vir	14.374	14.671	4.973 737	829.464 70	558361278143	5_5	4,15	
OGLE-LMC-T2CEP-095	5:20:09.84	−68:18:35.3	W Vir	17.009	17.873	5.000 122	2121.240 28	558353571684	7_5	4,14	(b); (f); (g); (h)
OGLE-LMC-T2CEP-087	5:18:21.64	−69:40:45.2	W Vir	16.887	17.770	5.184 979	454.045 23	558355510541	6_4	11,23	
OGLE-LMC-T2CEP-023	5:00:13.00	−67:42:43.7	pW Vir	15.511	16.101	5.234 801	2163.878 39	558351399660	7_3	4,16	
OGLE-LMC-T2CEP-083	5:16:58.99	−69:51:19.3	pW Vir	16.531	17.320	5.967 650	2119.656 83	558355634988	6_4	4,14	
OGLE-LMC-T2CEP-062	5:13:19.12	−69:38:57.6	W Vir	17.338	18.490	6.046 676	453.313 05	558355513592	6_4	4,14	(b); (e)
OGLE-LMC-T2CEP-133	5:29:23.48	−70:24:28.5	W Vir	16.671	17.497	6.281 955	2162.687 87	558361447993	5_5	4,15	
OGLE-LMC-T2CEP-137	5:30:03.55	−69:38:02.8	W Vir	16.728	17.633	6.362 350	453.960 88	558356644891	6_5	7,9	
OGLE-LMC-T2CEP-183	5:44:32.99	−69:48:21.8	W Vir	17.293	18.600	6.509 627	2183.465 56	558357893157	6_6	5,13	
OGLE-LMC-T2CEP-043	5:06:00.44	−69:55:14.6	W Vir	16.851	17.774	6.559 427	462.418 32	558355727258	6_4	4,14	(b); (f); (e); (g); (h)
OGLE-LMC-T2CEP-159	5:36:42.13	−69:31:11.7	W Vir	16.805	17.769	6.625 570	2182.537 72	558357684253	6_6	5,14	
OGLE-LMC-T2CEP-117	5:24:41.50	−71:06:44.6	W Vir	16.640	17.539	6.629 349	2165.529 37	558361934091	5_5	4,15	
OGLE-LMC-T2CEP-106	5:22:02.03	−69:27:25.3	W Vir	16.612	17.493	6.706 736	455.584 83	558356498352	6_5	7,9	
OGLE-LMC-T2CEP-078	5:16:29.09	−69:24:09.0	pW Vir	16.308	17.206	6.716 294	455.317 68	558355301964	6_4	4,14	
OGLE-LMC-T2CEP-063	5:13:43.86	−69:50:41.1	W Vir	16.662	17.553	6.924 580	2165.500 32	558355642907	6_4	4,14	
OGLE-LMC-T2CEP-110	5:22:19.48	−68:53:50.0	W Vir	16.763	17.705	7.078 468	2151.910 51	558356071179	6_5	7,9	
OGLE-LMC-T2CEP-181	5:43:37.42	−70:38:04.9	pW Vir	16.193	16.972	7.212 532	724.380 26	558360373616	5_7	4,8	
OGLE-LMC-T2CEP-047	5:07:46.53	−69:37:00.3	W Vir	16.616	17.536	7.286 212	723.500 42	558355524174	6_4	4,14	
OGLE-LMC-T2CEP-056	5:11:19.35	−69:34:32.3	W Vir	16.677	17.654	7.289 638	452.879 68	558355469354	6_4	4,14	
OGLE-LMC-T2CEP-100	5:21:14.64	−70:23:15.4	W Vir	16.642	17.407	7.431 095	825.702 18	558361448406	5_5	4,15	
OGLE-LMC-T2CEP-111	5:22:22.30	−70:52:46.8	W Vir	16.542	17.440	7.495 684	829.557 73	558361794595	5_5	4,15	

Table 2 – *continued*

ID	RA J2000	Dec. J2000	Type	$\langle I \rangle$ (mag)	$\langle V \rangle$ (mag)	Period (d)	Epoch (d)	VMC-ID	Tile	$N_{\rm Epochs}$ J,$K_{\rm s}$	Notes
(1)	(2)	(3)	(4)	(5)	(6)	(7)	(8)	(9)	(10)	(11)	(12)
OGLE-LMC-T2CEP-170	5:39:38.12	−68:48:24.9	W Vir	16.703	−99.990	7.682 906	2181.190 87	558357268116	6_6	5,14	(i)
OGLE-LMC-T2CEP-151	5:34:35.73	−69:59:14.9	W Vir	16.479	17.384	7.887 246	455.117 56	558358035015	6_6	5,14	
OGLE-LMC-T2CEP-179	5:43:04.02	−70:01:33.6	W Vir	16.744	17.805	8.050 065	2185.448 13	558358064065	6_6	4,14	
OGLE-LMC-T2CEP-182	5:43:46.89	−70:42:36.5	W Vir	16.312	17.265	8.226 419	2188.390 82	558360430553	5_7	4,8	
OGLE-LMC-T2CEP-094	5:19:53.20	−69:53:09.9	W Vir	16.588	17.529	8.468 490	2120.738 41	558356923555	6_5	7,9	
OGLE-LMC-T2CEP-019	4:58:49.42	−68:04:27.8	pW Vir	15.989	16.853	8.674 863	2162.749 38	558351644677	7_3	4,16	
OGLE-LMC-T2CEP-039	5:05:11.31	−67:12:45.3	W Vir	16.322	17.192	8.715 837	2166.319 77	558351083913	7_3	4,16	
OGLE-LMC-T2CEP-028	5:03:00.85	−70:07:33.7	pW Vir	15.543	16.045	8.784 807	2168.948 00	558358668771	5_3	4,9	
OGLE-LMC-T2CEP-074	5:15:48.75	−68:48:48.1	W Vir	16.070	16.892	8.988 344	2123.389 75	558354851839	6_4	4,14	
OGLE-LMC-T2CEP-152	5:34:37.58	−70:01:08.5	W Vir	16.453	17.323	9.314 921	453.026 63	558358053632	6_6	5,14	
OGLE-LMC-T2CEP-021	4:59:34.97	−71:15:31.2	pW Vir	15.884	16.580	9.759 502	2161.102 77	558359420632	5_3	4,11	
OGLE-LMC-T2CEP-132	5:29:08.23	−69:56:04.3	pW Vir	15.818	16.548	10.017 829	448.218 17	558356939981	6_5	7,9	
OGLE-LMC-T2CEP-146	5:31:48.01	−68:49:12.1	W Vir	16.392	17.347	10.079 593	2161.817 03	558357277233	6_6	12,23	
OGLE-LMC-T2CEP-097	5:20:20.58	−69:12:20.9	W Vir	16.177	17.064	10.510 167	446.108 16	558356294442	6_5	7,9	
OGLE-LMC-T2CEP-022	4:59:58.56	−70:34:27.8	W Vir	16.271	17.179	10.716 780	2157.787 14	558359020369	5_3	4,11	
OGLE-LMC-T2CEP-201	5:15:12.67	−69:13:08.0	pW Vir	14.611	15.152	11.007 243	456.113 01	558355159487	6_4	4,14	
OGLE-LMC-T2CEP-101	5:21:18.87	−69:11:47.3	W Vir	16.035	16.838	11.418 560	444.882 81	558356283672	6_5	7,9	
OGLE-LMC-T2CEP-013	4:55:24.41	−69:55:43.4	W Vir	16.184	17.119	11.544 611	2157.451 85	558358587418	5_3	4,11	
OGLE-LMC-T2CEP-178	5:42:19.01	−70:24:08.1	W Vir	16.326	17.406	12.212 367	726.431 60	558360198448	5_7	4,8	
OGLE-LMC-T2CEP-127	5:27:59.80	−69:23:27.5	W Vir	16.120	17.092	12.669 118	454.171 11	558356420696	6_5	7,9	
OGLE-LMC-T2CEP-118	5:25:15.05	−68:09:11.7	W Vir	16.103	17.037	12.698 580	2163.344 77	558353477576	7_5	4,14	
OGLE-LMC-T2CEP-103	5:21:35.27	−70:13:25.7	W Vir	16.039	16.995	12.908 278	824.386 16	558361309970	5_5	4,15	
OGLE-LMC-T2CEP-044	5:06:28.86	−69:43:58.8	W Vir	16.099	17.108	13.270 100	464.577 26	558355611443	6_4	4,14	
OGLE-LMC-T2CEP-026	5:02:11.56	−68:20:16.0	W Vir	16.091	17.026	13.577 869	2156.872 52	558351786614	7_3	4,16	
OGLE-LMC-T2CEP-096	5:20:10.42	−68:48:39.2	W Vir	15.918	16.832	13.925 722	2129.223 74	558356025075	6_5	7,9	
OGLE-LMC-T2CEP-157	5:36:02.60	−69:27:16.1	W Vir	16.045	17.050	14.334 647	2181.193 12	558357639701	6_6	5,14	
OGLE-LMC-T2CEP-017	4:56:16.02	−68:16:16.4	W Vir	15.986	16.968	14.454 754	2157.707 44	558351791598	7_3	4,16	
OGLE-LMC-T2CEP-143	5:31:09.75	−69:15:48.9	W Vir	15.806	16.701	14.570 185	2166.573 16	558356313034	6_5	12,23	
OGLE-LMC-T2CEP-046	5:07:38.94	−68:20:05.9	W Vir	15.547	16.415	14.743 796	2162.697 05	558351740940	7_3	4,16	(b); (c); (d); (f)
OGLE-LMC-T2CEP-139	5:30:22.56	−69:09:12.1	W Vir	15.968	17.003	14.780 410	2156.199 00	558356235708	6_5	7,9	
OGLE-LMC-T2CEP-177	5:40:36.54	−69:13:04.3	W Vir	16.132	17.240	15.035 903	2178.318 37	558357492207	6_6	5,14	
OGLE-LMC-T2CEP-099	5:20:44.48	−69:01:48.4	W Vir	15.932	16.999	15.486 788	2111.721 12	558356167163	6_5	7,9	
OGLE-LMC-T2CEP-086	5:18:17.80	−69:43:27.7	W Vir	15.629	16.486	15.845 500	452.844 78	558355544575	6_4	11,23	
OGLE-LMC-T2CEP-126	5:27:53.42	−70:51:30.9	W Vir	16.210	17.436	16.326 778	2167.506 61	558361770086	5_5	4,15	
OGLE-LMC-T2CEP-057	5:11:21.13	−68:40:13.3	W Vir	15.749	16.707	16.632 041	2159.167 41	558354781673	6_4	4,14	
OGLE-LMC-T2CEP-093	5:19:26.45	−69:51:51.0	W Vir	15.130	15.861	17.593 049	446.066 33	558356904142	6_5	7,9	(j)
OGLE-LMC-T2CEP-128	5:28:43.81	−70:14:02.3	W Vir	15.517	16.460	18.492 694	453.208 28	558361300181	5_5	4,15	
OGLE-LMC-T2CEP-058	5:11:33.52	−68:35:53.7	RV Tau	15.511	16.594	21.482 951	2167.453 98	558354737426	6_4	4,14	
OGLE-LMC-T2CEP-104	5:21:49.10	−70:04:34.3	RV Tau	14.937	15.830	24.879 948	447.757 45	558361170450	5_5	11,24	
OGLE-LMC-T2CEP-115	5:23:43.53	−69:32:06.8	RV Tau	15.593	16.651	24.966 913	2145.848 89	558356566155	6_5	7,9	
OGLE-LMC-T2CEP-192	5:53:55.69	−70:17:11.4	RV Tau	15.233	16.148	26.194 001	2181.449 82	558360150098	5_7	4,8	
OGLE-LMC-T2CEP-135	5:29:38.50	−69:15:12.2	RV Tau	15.194	16.162	26.522 364	2144.300 37	558356308540	6_5	7,9	
OGLE-LMC-T2CEP-108	5:22:11.27	−68:11:31.3	RV Tau	14.746	15.477	30.010 843	2113.813 36	558353504910	7_5	4,14	(k)
OGLE-LMC-T2CEP-162	5:37:44.95	−69:54:16.5	RV Tau	15.112	16.200	30.394 148	706.209 90	558357961649	6_6	5,14	
OGLE-LMC-T2CEP-180	5:43:12.87	−68:33:57.1	RV Tau	14.502	15.303	30.996 315	2178.207 91	558352877374	7_7	4,8	
OGLE-LMC-T2CEP-119	5:25:19.48	−70:54:10.0	RV Tau	14.391	15.225	33.825 094	2158.593 49	558361803554	5_5	4,15	
OGLE-LMC-T2CEP-050	5:09:26.15	−68:50:05.0	RV Tau	14.964	15.661	34.748 344	713.647 55	558354903269	6_4	4,14	
OGLE-LMC-T2CEP-200	5:13:56.43	−69:31:58.3	RV Tau	15.092	16.124	34.916 555	423.706 70	558355423319	6_4	4,14	(k)
OGLE-LMC-T2CEP-065	5:14:00.75	−68:57:56.8	RV Tau	14.699	15.611	35.054 940	455.175 14	558354970692	6_4	4,14	(k)
OGLE-LMC-T2CEP-091	5:18:45.48	−69:03:21.6	RV Tau	14.203	14.899	35.749 346	425.386 22	558355015602	6_4	11,23	
OGLE-LMC-T2CEP-203	5:22:33.79	−69:38:08.5	RV Tau	15.395	16.723	37.126 746	448.749 61	558356665485	6_5	7,9	
OGLE-LMC-T2CEP-202	5:21:49.09	−70:46:01.4	RV Tau	15.167	16.359	38.135 567	812.559 23	558361722614	5_5	4,15	
OGLE-LMC-T2CEP-112	5:22:58.36	−69:26:20.9	RV Tau	14.065	14.749	39.397 704	421.634 29	558356478674	6_5	7,9	
OGLE-LMC-T2CEP-051	5:09:41.93	−68:51:25.0	RV Tau	14.569	15.440	40.606 400	720.056 75	558354917278	6_4	4,14	(k)
OGLE-LMC-T2CEP-080	5:16:47.43	−69:44:15.1	RV Tau	14.341	15.175	40.916 413	436.421 11	558355560379	6_4	4,14	
OGLE-LMC-T2CEP-149	5:32:54.46	−69:35:13.2	RV Tau	14.151	14.868	42.480 613	2149.996 73	558357730269	6_6	5,14	
OGLE-LMC-T2CEP-032	5:03:56.31	−67:27:24.6	RV Tau	14.011	14.992	44.561 195	2152.876 23	558351226498	7_3	4,16	
OGLE-LMC-T2CEP-147	5:31:51.00	−69:11:46.3	RV Tau	13.678	14.391	46.795 842	2135.147 58	558357481187	6_6	9,23	
OGLE-LMC-T2CEP-174	5:40:00.50	−69:42:14.7	RV Tau	13.693	14.457	46.818 956	2166.799 27	558357814883	6_6	5,14	
OGLE-LMC-T2CEP-067	5:14:18.11	−69:12:35.0	RV Tau	13.825	14.627	48.231 705	442.942 73	558355160313	6_4	4,14	
OGLE-LMC-T2CEP-075	5:16:16.06	−69:43:36.9	RV Tau	14.568	15.728	50.186 569	430.990 79	558355554309	6_4	4,14	
OGLE-LMC-T2CEP-014	4:55:35.40	−69:54:04.2	RV Tau	14.312	15.103	61.875 713	2161.688 72	558358564467	5_3	4,11	(k)
OGLE-LMC-T2CEP-129	5:28:54.60	−69:52:41.1	RV Tau	14.096	14.813	62.508 947	397.727 80	558356885794	6_5	7,9	
OGLE-LMC-T2CEP-045	5:06:34.06	−69:30:03.7	RV Tau	13.729	14.787	63.386 339	2148.644 83	558355447114	6_4	4,14	

(a) Large separation (> 0.5 arcsec) between VMC and OGLE III star centroids likely due to crowding; (b) blended object; (c) faint object; (d) poor light curve; (e) very low amplitude in the optical; (f) source lies within a strip of the tile that has half the exposure of most of the tile (see Cross et al. 2012); (g) poorly sampled or heavily dispersed light curve (due to e.g. blending, saturation); (h) source image comes partly from detector 16 (on the top half of detector 16, the quantum ei¨ı $\frac{1}{2}$ fficiency varies on short time-scales making flat-fields inaccurate; Cross et al. 2012); (i) missing OGLE V magnitude; (j) light curve showing pulsation plus eclipse according to OGLE III; (k) correction for saturation not effective.

known LMC populations of the three different variable classes, respectively.

The OGLE III catalogues of T2CEP variables were cross-correlated against the VMC catalogue to obtain the J and K_s light curves for these variables. All the 130 T2CEPs were found to have a counterpart in the VMC catalogue within 2 arcsec from the OGLE III positions. The great majority of the objects showed separation in position with respect to OGLE III less than 0.1 arcsec. However, eight stars (OGLE-LMC-T2CEP-020, 030, 069, 084, 123, 142, 144, 173) present separations significantly larger than average (> 0.5 arcsec). Fig. 2 shows the OGLE III and VMC finding charts of 29 stars with some kind of identification or data problem, within which we included the eight objects quoted above. It can be seen that all the stars lie in crowded regions or are clearly blended by other stars or diffuse objects (e.g. OGLE-LMC-T2CEP-142). We will discuss these objects further in the following sections.

2.1 T2CEP light curves

The VMC time-series J and K_s photometry for the 130 objects is provided in Table 3, which is published in its entirety in the online version of the paper.

Periods and epochs of maximum light available from the OGLE III catalogue were used to fold the J- and K_s-band light curves produced by the VMC observations. Given the larger number of epochs in K_s with respect to J, we discuss first the K_s-band data.

The K_s-band light curves for a sample of 120 T2CEPs with useful light curves are shown in Fig. A1. Apart from a few cases, these light curves are generally well sampled and nicely shaped. Some clearly discrepant data points (open circles in Fig. A1) in the light curves were excluded from the fit but were plotted in the figure for completeness. Note that most of these 'bad' data points belong to observations collected during nights that did not strictly meet the VMC observing constraints (see table 2 in Cioni et al. 2011). The final spline fit to the data is shown by a solid line in Fig. A1. Intensity-averaged $\langle K_s \rangle$ magnitudes were derived from the light curves using custom software written in C, which performs a spline interpolation to the data with no need of using templates. The numerical model of the light curve is thus obtained and then integrated in intensity to obtain the mean intensity which is eventually transformed to mean magnitude.

10 objects in our sample showed unusable light curves, namely OGLE-LMC-T2CEP-014, 030, 043, 051, 065, 084, 095, 108, 142 and 200. Their light curves are displayed in Fig. A2, whereas their finding charts are shown in Fig. 2. A quick analysis of the finding charts reveals that all these stars have significant problems of crowding/blending. Three of the aforementioned objects (OGLE-LMC-T2CEP-030, 084 and 142) have centroids significantly shifted with respect to OGLE's, thus confirming the presence of strong blending.

As for the J-band data, Fig. A3 shows the light curves for the 34 stars that have sufficiently good data to allow an independent spline fit (solid line in the figure). Figs A4 and A5 show the light curves for the remaining 86 and 10 objects with small number of epochs (∼4–5 on average) and dispersed light curves, respectively. The latter variables show the same problems reported for the K_s band. To estimate the intensity-averaged J magnitude for the 86 stars possessing only few epochs of observation, we decided to use the spline-fit curves in the K_s band as templates.[5] To this aim, for each star we performed the following steps: (1) subtracted the average $\langle K_s \rangle$ magnitude from the K_s spline-fit curve; (2) adjusted by eye the data obtained in this way to fit the J light curve by (i) adding a ZP, (ii) multiplying the amplitude by a proper factor and (iii) shifting the light curve in phase. The factor needed for point (ii) is the ratio Amp(J)/Amp(K_s). To estimate this number, we used the 34 stars with independent J-band spline fit, obtaining a value of 1.1 ± 0.2. The uncertainty of ∼20 per cent may appear large, but it does not actually represent a problem since its contribution to the error on the intensity-averaged J is of the order of 0.5 per cent. In some favourable cases, the few data points covered both maximum and minimum of the light curve and it was then possible to constrain directly the amplitude ratio. The shift in phase (point iii above) varied from case to case, but was on average close to 0.05–0.06. The final error on the intensity-averaged J magnitude was calculated by summing in quadrature the error on the K_s magnitude, the uncertainty on the J magnitude caused by the error on the amplitude ratio and an additional 1 per cent to take into account the uncertainty on the phase shift. The goodness of this procedure can be appreciated in Fig. 3, where we show in different colours the PL and PW relations (see the next section for a detailed description of these relations) for the stars with intensity-averaged J photometry obtained directly from spline fits (black points) and with the template fits (grey points). The figure clearly shows that the results obtained on the basis of the K_s templates are usable for scientific purposes. The final $\langle J \rangle$,$\langle K_s \rangle$ magnitudes with relative uncertainties, as well as pulsational amplitudes and adopted reddening values (see Section 3), are provided in Table 4.

We recall that the J and K_s photometry presented in this paper is set in the VISTA system. A consistent comparison between our results and those in the widely used 2MASS system (Two Micron All Sky Survey; Skrutskie et al. 1996) can be performed after applying proper system transformations as for instance those provided by the Cambridge Astronomy Survey Unit (CASU):[6] $(J - K_s)(\mathrm{2MASS}) = 1.081(J - K_s)(\mathrm{VISTA})$, $J(\mathrm{2MASS}) = J(\mathrm{VISTA}) + 0.07(J - K_s)(\mathrm{VISTA})$ and $K_s(\mathrm{2MASS}) = K_s(\mathrm{VISTA}) - 0.011(J - K_s)(\mathrm{VISTA})$.

Since the $\langle J \rangle - \langle K_s \rangle$ colour of our T2CEP sample typically ranges from 0.1 to 0.6 mag, the VISTA and 2MASS K_s can be considered equivalent for T2CEPs (see Fig. 4) and for CCs (see Ripepi et al. 2012b), to a very good approximation (better than ∼5 mmag).

3 J-, K_s-BAND PL, PLC AND PW RELATIONS

The data reported in Table 4 allow us to calculate different useful relationships adopting various combinations of magnitudes and colours. In particular, we derived PL relations in J and K_s as well as PW and PLC relations for the following combinations: (J, $V - J$), (K_s,$V - K_s$) and (K_s,$J - K_s$).

We first corrected magnitudes and colours for reddening using the recent extinction maps by Haschke, Grebel & Duffau (2011). Individual $E(V - I)$ reddening values for the 120 T2CEPs with useful VMC data are reported in column 10 of Table 4. The reliability of this reddening correction can be questioned by observing that it has been derived from the analysis of the red clump stars, which trace the intermediate-age population (2–9 Gyr)

[5] A comparison of Fig. A1 (K_s light curves) and A3 (J light curves for stars possessing sufficient data points to be analysed independently from the K_s band) shows that at present level of precision, the light curves in J and K_s are sufficiently similar to allow us using the K_s spline fits as templates.

[6] http://casu.ast.cam.ac.uk/surveys-projects/vista/technical/photometric-properties

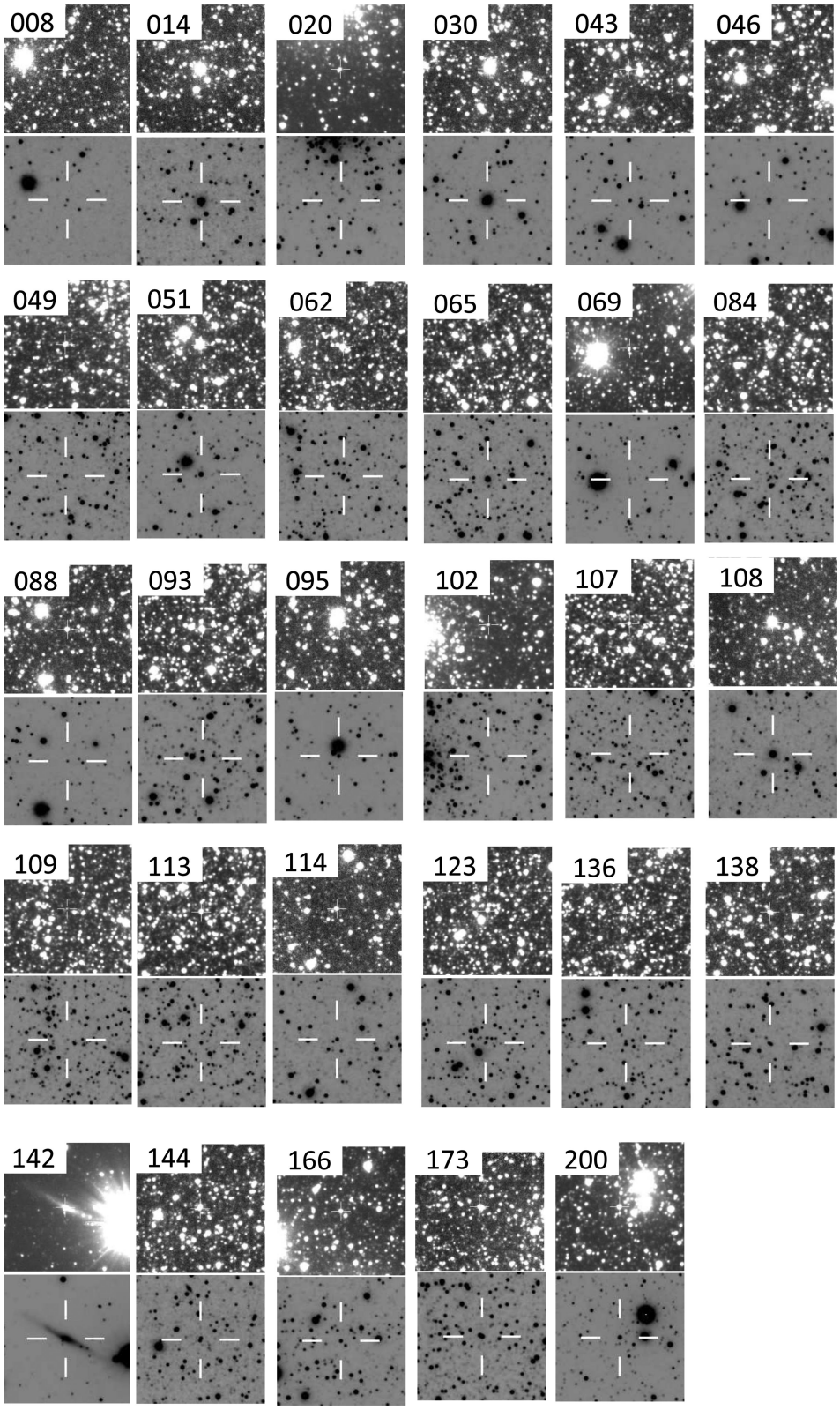

Figure 2. Sky pictures for 29 problematic stars extracted from the VMC (bottom panels) and the OGLE III (top panels) archives. The target is identified with the last three digits of the OGLE III identification (i.e. without the prefix 'OGLE-LMC-T2CEP-').

instead of the old one to whom BL Her and W Vir belong. However, we recall that in the NIR bands the interstellar absorption is very low: $A_J \sim 0.25A_V$ and $A_{K_s} \sim 0.1A_V$, where A_V is the absorption in the visible. Hence, even in the unlikely case of a 10 per cent large error in our A_V estimates, this would introduce an amount of uncertainties of only ∼2.5 per cent and ∼1 per cent in J and K_s, respectively. An a posteriori indication about the global correctness of the adopted reddening correction is represented by the

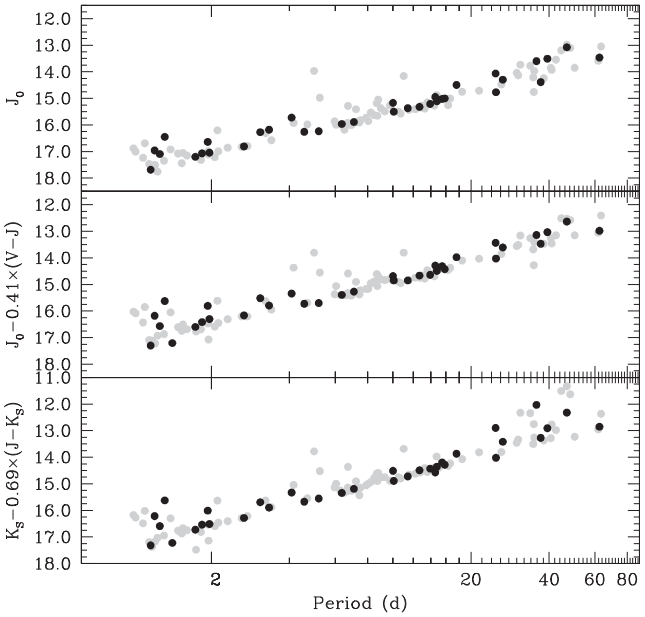

Figure 3. From top to bottom: PL in the J band, PW in $(J, V-J)$ and PW in $(K_s, J-K_s)$ for T2CEPs whose intensity-averaged $\langle J\rangle$ magnitude was obtained on the basis of direct spline fit (black filled circles) or template fit (grey filled circles). See the text for details.

Table 3. J and K_s time-series photometry for the T2CEPs investigated in this paper. The data below refer to the variable OGLE-LMC-T2CEP-123.

HJD−2400000	J	σ_J
55487.77111	16.963	0.014
55487.80976	16.959	0.014
55497.79317	16.989	0.014
55497.86048	16.950	0.013
HJD−2400000	K_s	σ_{K_s}
55495.82644	16.520	0.020
55497.75937	16.520	0.020
55497.81507	16.513	0.024
55499.82170	16.517	0.023
55511.74774	16.507	0.020
55516.77236	16.496	0.023
55526.78868	16.498	0.021
55539.82483	16.488	0.022
55557.73937	16.482	0.023
55563.71325	16.465	0.021
55587.65755	16.470	0.023
55844.79771	16.526	0.020
55865.82753	16.483	0.021
55887.74744	16.477	0.022
55937.67877	16.454	0.021

Table 3 is published in its entirety only in the electronic edition of the journal. A portion is shown here for guidance regarding its form and content.

concordance of results provided by the PL (reddening-dependent) and PW (reddening-independent) relations (see Sections 4 and 5). The reddening values were converted using the following equations: $E(V-J) = 1.80E(V-I)$, $E(V-K_s) = 2.24E(V-I)$ and

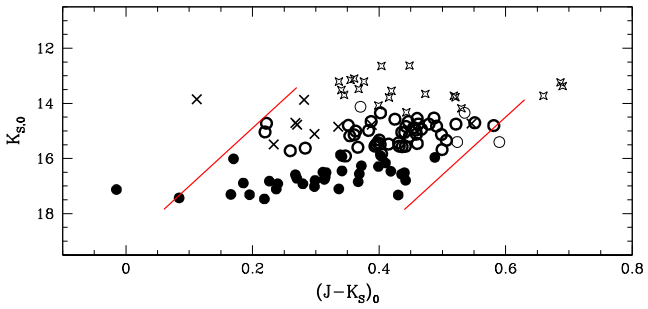

Figure 4. Observed instability strip in the plane $K_{s,0}$ versus $(J-K_s)_0$. Filled circles, open circles, crosses and stars show BL Her, W Vir, pW Vir and RV Tau variables, respectively. The solid lines show the approximate borders of the BL Her/W Vir instability strip. Blue and red edges are described by the following equations: $K_{s,0} = 19.1-21(J-K_s)_0$ $(0.06 < (J-K_s)_0 < 0.27$ mag) and $K_{s,0} = 27.1-21(J-K_s)_0$ $(0.44 < (J-K_s)_0 < 0.63$ mag), respectively.

$E(J-K_s) = 0.43E(V-I)$ (Cardelli, Clayton & Mathis 1989; Gao et al. 2013).[7] The coefficients of the PW relations were calculated in a similar way.

In principle, an additional preliminary step would be required, i.e. the correction for the inclination of the LMC disc-like structure by de-projecting each T2CEP with respect to the LMC centre. To do this, we followed the procedure suggested in van der Marel & Cioni (2001) and adopted their values of the LMC centre, inclination and position angle of the line of nodes. However, we have a posteriori verified that the introduction of this correction leads to worse results, i.e. larger dispersion in the various relationships mentioned above. To verify if different choices about the inclined disc parameters could improve the results, we have carried out the de-projection using several results present in the literature (see Haschke et al. 2012; Rubele et al. 2012; Subramanian & Subramaniam 2013, and references therein). Under no circumstances, the dispersion of the PWs decreased (we used PWs as reference because they are reddening-free). To explain this occurrence, we can reasonably hypothesize that the T2CEPs (actually BL Her and W Vir), being old (age$>$ 10 Gyr) objects, are not preferentially distributed along the main disc-like structure of the LMC. Alternatively, the adopted parameters for the de-projection are not accurate enough, although this conclusion may be influenced by the relatively small number of objects. Subsequent studies using a larger number of objects observed in the VMC context sampling different populations (CCs, T2CEPs and RR Lyrae stars) will clarify the issue. In any case, in the following analysis we did not apply any magnitude correction accounting for the LMC disc structure.

Figs 5–8 show all the relationships investigated here. An inspection of these figures confirms the findings by Matsunaga et al. (2009) that BL Her and W Vir star follow a common PL relation, whereas RV Tau show a different and more dispersed relation (the dispersion is less severe in the J than in the K_s band). In our case, the dispersion among RV Tau stars can in part be due to the proximity of several bright variables to the saturation limit. As a consequence, we decided to exclude these stars from the calculation of the PL, PW and PLC relations. To check if BL Her and W Vir stars can actually be fitted with a unique relation, we performed an independent test by fitting separately the PL(K_s, J) and PW(K_s, V) relations for each class of variables. The result of this exercise is shown in Fig. 9: for

[7] The coefficients we used are suited for the 2MASS system, to which the VISTA system is tied (see Section 2.1).

Table 4. Results for the 120 T2CEPs with useful NIR light curves analysed in this paper. The columns report (1) OGLE identification; (2) variability class; (3) period (OGLE); (4) intensity-averaged J magnitude; (5) uncertainty on the $\langle J \rangle$ (6) intensity-averaged K_s magnitude; (7) uncertainty on the $\langle K_s \rangle$; (8) peak-to-peak amplitude in J; (9) peak-to-peak amplitude in K_s; (10) adopted reddening; (11) T = results in J obtained on the basis of the K_s template, S = results in J obtained on the basis of direct spline fitting to the data.

ID	Var. class	Period (d)	$\langle J \rangle$ (mag)	$\sigma_{\langle J \rangle}$ (mag)	$\langle K_s \rangle$ (mag)	$\sigma_{\langle K_s \rangle}$ (mag)	Amp(J) (mag)	Amp(K_s) (mag)	$E(V-I)$ (mag)	Note
(1)	(2)	(3)	(4)	(5)	(6)	(7)	(8)	(9)	(10)	(11)
OGLE-LMC-T2CEP-123	BL Her	1.002 6263	16.939	0.021	16.486	0.013	0.05	0.05	0.080	T
OGLE-LMC-T2CEP-069	BL Her	1.021 2542	17.042	0.033	16.585	0.021	0.10	0.10	0.050	T
OGLE-LMC-T2CEP-114	BL Her	1.091 0886	17.329	0.069	16.831	0.019	0.17	0.16	0.130	T
OGLE-LMC-T2CEP-020	BL Her	1.108 1258	16.735	0.043	16.310	0.022	0.09	0.07	0.060	T
OGLE-LMC-T2CEP-071	BL Her	1.152 1638	17.522	0.022	17.326	0.026	0.40	0.38	0.070	T
OGLE-LMC-T2CEP-089	BL Her	1.167 2977	17.715	0.018	17.479	0.043	0.40	0.32	0.040	S
OGLE-LMC-T2CEP-061	BL Her	1.181 5124	17.581	0.037	17.458	0.031	0.38	0.19	0.090	T
OGLE-LMC-T2CEP-107	BL Her	1.209 1451	16.979	0.005	16.526	0.016	0.19	0.13	0.030	S
OGLE-LMC-T2CEP-077	BL Her	1.213 8023	17.521	0.045	17.317	0.025	0.18	0.17	0.020	T
OGLE-LMC-T2CEP-165	BL Her	1.240 8330	17.889	0.049	17.381	0.024	0.34	0.32	0.180	T
OGLE-LMC-T2CEP-102	BL Her	1.266 0176	17.146	0.010	16.817	0.020	0.20	0.13	0.070	S
OGLE-LMC-T2CEP-194	BL Her	1.314 4675	17.406	0.017	17.134	0.018	0.38	0.24	0.080	T
OGLE-LMC-T2CEP-136	BL Her	1.323 0384	16.492	0.011	15.978	0.006	0.31	0.08	0.060	S
OGLE-LMC-T2CEP-138	BL Her	1.393 5906	16.975	0.043	16.576	0.017	0.07	0.07	0.070	T
OGLE-LMC-T2CEP-109	BL Her	1.414 5528	18.610	0.056	17.790	0.038	0.43	0.38	0.030	S
OGLE-LMC-T2CEP-105	BL Her	1.489 2979	17.134	0.012	16.914	0.021	0.41	0.27	0.080	T
OGLE-LMC-T2CEP-122	BL Her	1.538 6690	17.520	0.034	17.136	0.018	0.24	0.23	0.110	T
OGLE-LMC-T2CEP-171	BL Her	1.554 7492	17.175	0.017	16.875	0.017	0.18	0.17	0.170	T
OGLE-LMC-T2CEP-068	BL Her	1.609 3007	17.225	0.028	16.942	0.018	0.27	0.26	0.100	T
OGLE-LMC-T2CEP-124	BL Her	1.734 8666	17.280	0.009	16.953	0.030	0.30	0.30	0.110	S
OGLE-LMC-T2CEP-008	BL Her	1.746 0989	17.257	0.023	17.389	0.028	0.08	0.08	0.100	T
OGLE-LMC-T2CEP-141	BL Her	1.822 9539	17.389	0.023	17.048	0.021	0.36	0.40	0.100	T
OGLE-LMC-T2CEP-140	BL Her	1.841 1435	17.127	0.012	16.779	0.014	0.21	0.27	0.080	S
OGLE-LMC-T2CEP-144	BL Her	1.937 4502	16.726	0.017	16.302	0.011	0.22	0.20	0.120	S
OGLE-LMC-T2CEP-130	BL Her	1.944 6935	17.036	0.016	16.740	0.021	0.36	0.34	0.060	T
OGLE-LMC-T2CEP-088	BL Her	1.950 7490	17.158	0.012	17.147	0.028	0.09	0.09	0.060	T
OGLE-LMC-T2CEP-116	BL Her	1.966 6793	17.086	0.038	16.746	0.007	0.23	0.32	0.060	S
OGLE-LMC-T2CEP-121	BL Her	2.061 3655	17.234	0.033	16.854	0.014	0.45	0.43	0.030	T
OGLE-LMC-T2CEP-166	BL Her	2.110 5987	16.343	0.015	15.922	0.006	0.23	0.22	0.190	T
OGLE-LMC-T2CEP-064	BL Her	2.127 8906	17.043	0.019	16.698	0.025	0.47	0.45	0.070	T
OGLE-LMC-T2CEP-167	BL Her	2.311 8238	17.091	0.045	16.685	0.010	0.50	0.48	0.320	T
OGLE-LMC-T2CEP-092	BL Her	2.616 7684	16.864	0.097	16.526	0.066	0.69	0.66	0.050	T
OGLE-LMC-T2CEP-148	BL Her	2.671 7338	16.853	0.011	16.516	0.015	0.43	0.56	0.060	S
OGLE-LMC-T2CEP-195	BL Her	2.752 9292	16.850	0.021	16.474	0.008	0.55	0.46	0.080	T
OGLE-LMC-T2CEP-113	BL Her	3.085 4602	16.285	0.002	15.935	0.008	0.10	0.06	0.020	S
OGLE-LMC-T2CEP-049	BL Her	3.235 2751	16.359	0.015	15.926	0.010	0.25	0.24	0.070	T
OGLE-LMC-T2CEP-145	BL Her	3.337 3019	16.269	0.008	16.047	0.015	0.11	0.08	0.120	S
OGLE-LMC-T2CEP-085	BL Her	3.405 0955	16.640	0.017	16.191	0.011	0.47	0.45	0.090	T
OGLE-LMC-T2CEP-134	pW Vir	4.075 7258	15.782	0.009	15.514	0.007	0.31	0.36	0.080	S
OGLE-LMC-T2CEP-173	W Vir	4.147 8811	16.049	0.018	15.452	0.005	0.12	0.11	0.170	T
OGLE-LMC-T2CEP-120	W Vir	4.559 0530	16.354	0.007	15.951	0.009	0.38	0.38	0.130	S
OGLE-LMC-T2CEP-052	pW Vir	4.687 9253	16.031	0.018	15.741	0.022	0.14	0.13	0.070	T
OGLE-LMC-T2CEP-098	pW Vir	4.973 7372	14.056	0.014	13.892	0.005	0.15	0.14	0.120	T
OGLE-LMC-T2CEP-087	W Vir	5.184 9790	16.302	0.013	15.859	0.015	0.30	0.31	0.090	S
OGLE-LMC-T2CEP-023	pW Vir	5.234 8007	15.005	0.043	14.720	0.013	0.36	0.34	0.040	T
OGLE-LMC-T2CEP-083	pW Vir	5.967 6496	15.936	0.054	15.462	0.011	0.48	0.46	0.100	T
OGLE-LMC-T2CEP-062	W Vir	6.046 6764	16.060	0.019	15.431	0.003	0.05	0.05	0.090	T
OGLE-LMC-T2CEP-133	W Vir	6.281 9551	16.013	0.010	15.564	0.013	0.09	0.09	0.040	T
OGLE-LMC-T2CEP-137	W Vir	6.362 3499	16.044	0.004	15.630	0.010	0.11	0.11	0.110	S
OGLE-LMC-T2CEP-183	W Vir	6.509 6275	16.325	0.016	15.739	0.016	0.15	0.14	0.200	T
OGLE-LMC-T2CEP-159	W Vir	6.625 5696	16.089	0.015	15.605	0.010	0.09	0.09	0.110	T
OGLE-LMC-T2CEP-117	W Vir	6.629 3487	16.007	0.012	15.579	0.005	0.12	0.11	0.080	T
OGLE-LMC-T2CEP-106	W Vir	6.706 7363	15.956	0.055	15.474	0.010	0.16	0.15	0.050	T
OGLE-LMC-T2CEP-078	pW Vir	6.716 2943	15.349	0.016	14.764	0.011	0.15	0.14	0.090	T
OGLE-LMC-T2CEP-063	W Vir	6.924 5800	16.040	0.023	15.577	0.016	0.14	0.13	0.050	T
OGLE-LMC-T2CEP-110	W Vir	7.078 4684	15.978	0.008	15.511	0.017	0.16	0.15	0.120	S
OGLE-LMC-T2CEP-181	pW Vir	7.212 5323	15.505	0.013	15.151	0.005	0.07	0.07	0.130	T
OGLE-LMC-T2CEP-047	W Vir	7.286 2123	15.943	0.018	15.511	0.011	0.14	0.13	0.070	T
OGLE-LMC-T2CEP-056	W Vir	7.289 6382	15.965	0.017	15.522	0.004	0.16	0.15	0.110	T

Table 4 – *continued*

ID	Var. class	Period (d)	$\langle J \rangle$ (mag)	$\sigma_{\langle J \rangle}$ (mag)	$\langle K_s \rangle$ (mag)	$\sigma_{\langle K_s \rangle}$ (mag)	Amp(J) (mag)	Amp(K_s) (mag)	$E(V-I)$ (mag)	Note
(1)	(2)	(3)	(4)	(5)	(6)	(7)	(8)	(9)	(10)	(11)
OGLE-LMC-T2CEP-100	W Vir	7.431 0950	15.965	0.012	15.647	0.020	0.29	0.28	0.080	T
OGLE-LMC-T2CEP-111	W Vir	7.495 6838	15.865	0.011	15.441	0.006	0.19	0.18	0.060	T
OGLE-LMC-T2CEP-170	W Vir	7.682 9062	15.926	0.018	15.423	0.004	0.16	0.15	0.180	T
OGLE-LMC-T2CEP-151	W Vir	7.887 2458	15.814	0.016	15.366	0.009	0.14	0.13	0.110	T
OGLE-LMC-T2CEP-179	W Vir	8.050 0650	15.932	0.014	15.378	0.005	0.14	0.13	0.110	T
OGLE-LMC-T2CEP-182	W Vir	8.226 4194	15.628	0.035	15.218	0.007	0.37	0.35	0.130	T
OGLE-LMC-T2CEP-094	W Vir	8.468 4897	15.659	0.048	15.143	0.006	0.10	0.10	0.040	T
OGLE-LMC-T2CEP-019	pW Vir	8.674 8634	15.263	0.024	14.880	0.015	0.33	0.31	0.110	T
OGLE-LMC-T2CEP-039	W Vir	8.715 8373	15.682	0.018	15.217	0.009	0.19	0.18	0.040	T
OGLE-LMC-T2CEP-028	pW Vir	8.784 8073	15.083	0.016	14.791	0.006	0.32	0.30	0.050	T
OGLE-LMC-T2CEP-074	W Vir	8.988 3439	15.414	0.019	15.025	0.025	0.22	0.21	0.060	T
OGLE-LMC-T2CEP-152	W Vir	9.314 9211	15.559	0.013	15.080	0.004	0.39	0.37	0.100	T
OGLE-LMC-T2CEP-021	pW Vir	9.759 5024	15.309	0.046	15.059	0.018	0.16	0.15	0.070	T
OGLE-LMC-T2CEP-132	pW Vir	10.017 8287	15.227	0.015	14.804	0.005	0.22	0.09	0.080	S
OGLE-LMC-T2CEP-146	W Vir	10.079 5925	15.576	0.026	15.172	0.021	0.37	0.29	0.100	S
OGLE-LMC-T2CEP-097	W Vir	10.510 1666	15.530	0.062	15.068	0.006	0.28	0.27	0.050	T
OGLE-LMC-T2CEP-022	W Vir	10.716 7800	15.598	0.011	15.126	0.015	0.35	0.33	0.030	T
OGLE-LMC-T2CEP-201	pW Vir	11.007 2431	14.195	0.018	13.892	0.007	0.06	0.06	0.050	T
OGLE-LMC-T2CEP-101	W Vir	11.418 5596	15.427	0.009	15.009	0.007	0.45	0.40	0.080	S
OGLE-LMC-T2CEP-013	W Vir	11.544 6113	15.498	0.014	15.001	0.013	0.22	0.21	0.090	T
OGLE-LMC-T2CEP-178	W Vir	12.212 3667	15.517	0.020	14.985	0.008	0.33	0.31	0.150	T
OGLE-LMC-T2CEP-127	W Vir	12.669 1185	15.372	0.022	14.851	0.011	0.48	0.37	0.070	S
OGLE-LMC-T2CEP-118	W Vir	12.698 5804	15.412	0.038	14.914	0.007	0.72	0.69	0.100	T
OGLE-LMC-T2CEP-103	W Vir	12.908 2775	15.336	0.011	14.859	0.019	0.40	0.38	0.080	T
OGLE-LMC-T2CEP-044	W Vir	13.270 1004	15.455	0.030	14.835	0.013	0.30	0.29	0.090	T
OGLE-LMC-T2CEP-026	W Vir	13.577 8689	15.209	0.089	14.823	0.012	0.39	0.37	0.080	T
OGLE-LMC-T2CEP-096	W Vir	13.925 7224	15.277	0.056	14.776	0.006	0.81	0.75	0.090	S
OGLE-LMC-T2CEP-157	W Vir	14.334 6466	15.304	0.045	14.782	0.043	0.66	0.63	0.100	T
OGLE-LMC-T2CEP-017	W Vir	14.454 7544	15.354	0.056	14.785	0.021	0.81	0.77	0.110	T
OGLE-LMC-T2CEP-143	W Vir	14.570 1846	14.991	0.075	14.743	0.068	1.05	0.72	0.060	S
OGLE-LMC-T2CEP-046	W Vir	14.743 7956	14.921	0.058	14.360	0.021	0.62	0.59	0.060	T
OGLE-LMC-T2CEP-139	W Vir	14.780 4104	15.220	0.014	14.709	0.005	0.50	0.51	0.150	S
OGLE-LMC-T2CEP-177	W Vir	15.035 9027	15.245	0.024	14.741	0.007	0.69	0.66	0.270	T
OGLE-LMC-T2CEP-099	W Vir	15.486 7877	15.094	0.003	14.564	0.005	0.51	0.52	0.100	S
OGLE-LMC-T2CEP-086	W Vir	15.845 5000	15.024	0.011	14.586	0.017	0.79	0.80	0.030	S
OGLE-LMC-T2CEP-126	W Vir	16.326 7785	15.323	0.023	14.733	0.013	0.77	0.73	0.090	T
OGLE-LMC-T2CEP-057	W Vir	16.632 0415	15.052	0.021	14.566	0.013	0.82	0.78	0.060	T
OGLE-LMC-T2CEP-093	W Vir	17.593 0492	14.524	0.021	14.136	0.019	0.61	0.47	0.040	S
OGLE-LMC-T2CEP-128	W Vir	18.492 6938	14.787	0.023	14.363	0.054	0.71	0.68	0.050	T
OGLE-LMC-T2CEP-058	RV Tau	21.482 9509	14.777	0.017	14.208	0.014	0.75	0.71	0.090	T
OGLE-LMC-T2CEP-104	RV Tau	24.879 9480	14.131	0.020	13.402	0.043	0.32	0.61	0.090	S
OGLE-LMC-T2CEP-115	RV Tau	24.966 9126	14.790	0.002	14.334	0.013	0.66	0.63	0.030	S
OGLE-LMC-T2CEP-192	RV Tau	26.194 0011	14.521	0.033	14.096	0.008	1.09	1.04	0.060	T
OGLE-LMC-T2CEP-135	RV Tau	26.522 3638	14.350	0.016	13.799	0.015	1.09	0.76	0.070	S
OGLE-LMC-T2CEP-162	RV Tau	30.394 1483	14.294	0.043	13.726	0.043	0.57	0.41	0.220	T
OGLE-LMC-T2CEP-180	RV Tau	30.996 3145	13.785	0.068	12.921	0.033	0.42	0.40	0.070	T
OGLE-LMC-T2CEP-119	RV Tau	33.825 0938	13.832	0.021	12.951	0.064	0.89	0.85	0.080	T
OGLE-LMC-T2CEP-050	RV Tau	34.748 3438	14.257	0.030	13.811	0.014	0.19	0.18	0.070	T
OGLE-LMC-T2CEP-091	RV Tau	35.749 3456	13.652	0.045	12.693	0.055	0.62	0.64	0.070	S
OGLE-LMC-T2CEP-203	RV Tau	37.126 7463	14.416	0.007	13.739	0.004	0.61	0.39	0.040	S
OGLE-LMC-T2CEP-202	RV Tau	38.135 5674	14.310	0.013	13.753	0.015	0.07	0.07	0.090	T
OGLE-LMC-T2CEP-112	RV Tau	39.397 7037	13.531	0.021	13.163	0.009	0.27	0.24	0.030	S
OGLE-LMC-T2CEP-080	RV Tau	40.916 4131	13.957	0.027	13.253	0.047	0.44	0.42	0.040	T
OGLE-LMC-T2CEP-149	RV Tau	42.480 6129	13.649	0.039	13.252	0.007	0.13	0.12	0.140	T
OGLE-LMC-T2CEP-032	RV Tau	44.561 1948	13.232	0.030	12.212	0.090	0.36	0.34	0.050	T
OGLE-LMC-T2CEP-147	RV Tau	46.795 8419	13.145	0.017	12.658	0.013	0.06	0.06	0.090	T
OGLE-LMC-T2CEP-174	RV Tau	46.818 9562	13.089	0.016	12.048	0.030	0.46	0.44	0.150	T
OGLE-LMC-T2CEP-067	RV Tau	48.231 7051	13.176	0.022	12.263	0.052	0.20	0.19	0.100	T
OGLE-LMC-T2CEP-075	RV Tau	50.186 5686	13.900	0.110	13.502	0.033	0.78	0.74	0.070	T
OGLE-LMC-T2CEP-129	RV Tau	62.508 9466	13.514	0.035	13.123	0.013	0.16	0.14	0.070	S
OGLE-LMC-T2CEP-045	RV Tau	63.386 3391	13.098	0.024	12.664	0.021	0.16	0.15	0.070	T

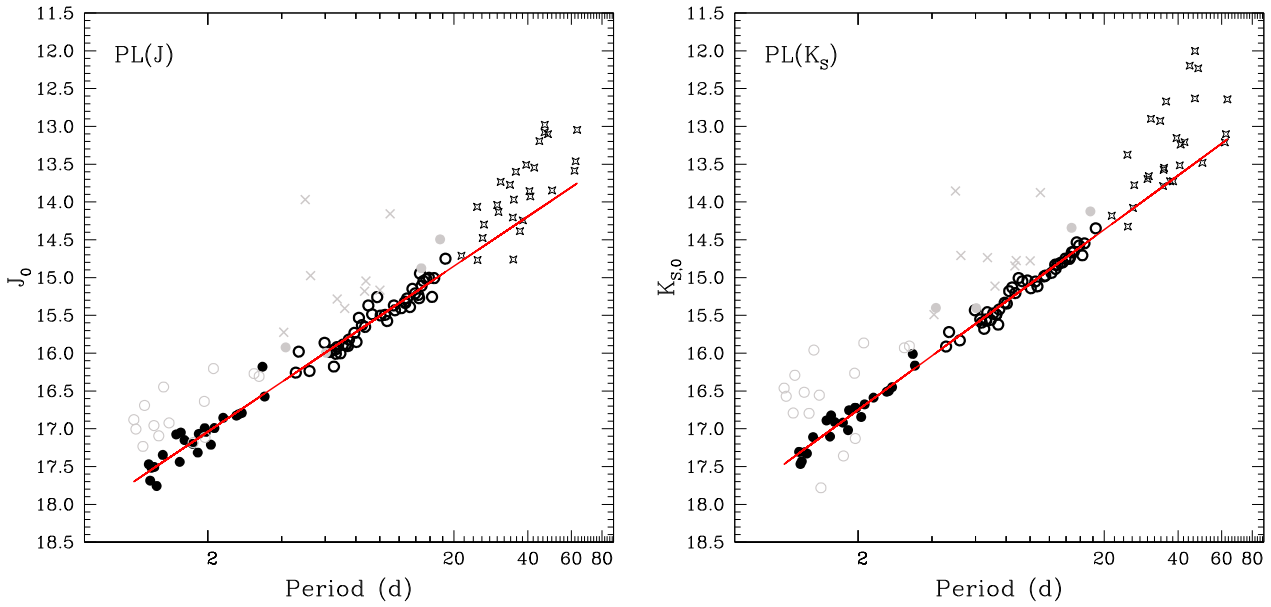

Figure 5. PL(J) and PL(K_s) relations for the T2CEPs investigated in this paper. The meaning of the symbols is the following: black filled and open circles are the BL Her and W Vir variables used in the derivation of the PL, PW and PLC relationships, respectively. Grey open and filled circles are the BL Her and W Vir variables discarded because of problems in the photometry (see the text). Grey crosses are the peculiar W Vir stars. The starred symbols represent the RV Tau variables. The size of the symbols is generally representative of the measurement errors. The solid lines represent the least-squares fit to the data shown in Table 5. We recall that RV Tau stars were not used in the calculation of the least-squares fits (see the text).

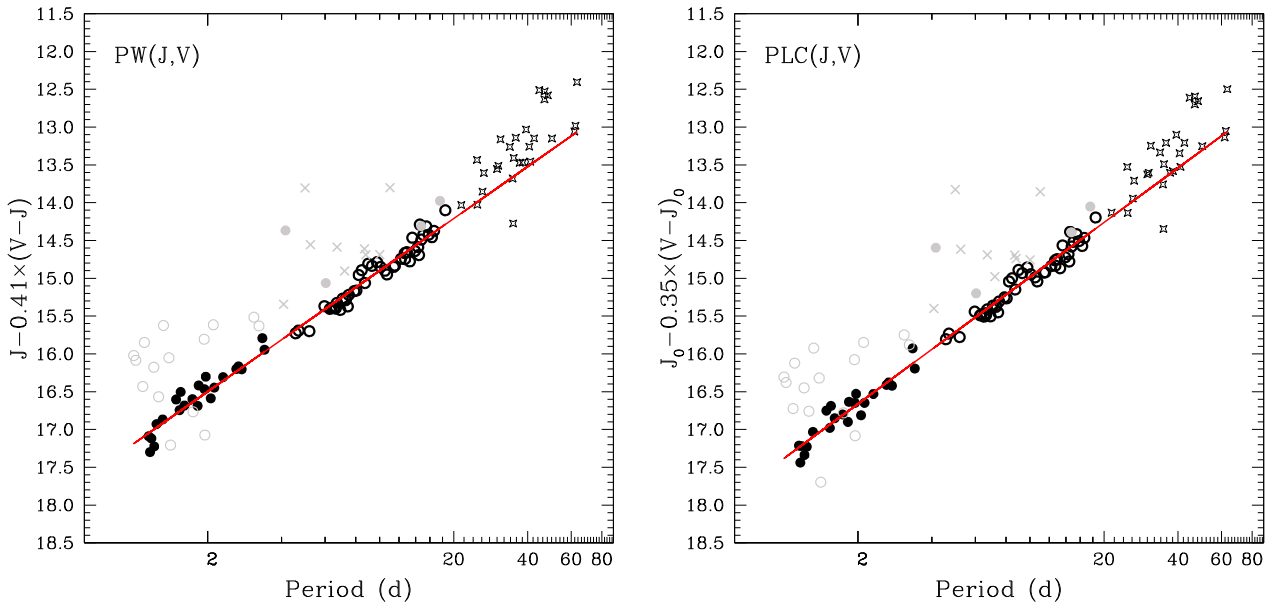

Figure 6. PW(J, V) and PLC(J, V) for the T2CEPs investigated in this paper. Symbols are as in Fig. 5.

both relations, the two variable classes seem to show results that agree with each other well within 1σ, thus confirming that we can use BL Her and W Vir variables together.

For each combination of periods, magnitudes and colours, we performed independent least-squares fits to the data, adopting equations of the form reported in Table 5. The results of the fitting procedure are shown in the same table as well as in Figs 5–8 with a solid line. Note that the equations listed in Table 5 are given in terms of absolute magnitudes since we subtracted the dereddened distance modulus ($DM_{0,\,LMC}$) of the LMC from each equation. Thus, the absolute ZP of the relations in Table 5 can be simply obtained by using the preferred value for the $DM_{0,\,LMC}$ value.

In deriving the equations of Table 5, we have implicitly neglected any dependence of both PL and PW relations on the metallicity of the pulsators. This is in agreement with Matsunaga et al. (2006), who found a hardly significant dependence of the PL relations on metallicity (0.1 ± 0.06 mag dex^{-1}), whereas the theoretical models by Di Criscienzo et al. (2007) predict a very mild metallicity dependence ΔMag/Δ [Fe/H]$\sim$0.04–0.06 mag dex^{-1} for both the PL and PW relations in the magnitudes and colours of interest. In any case, the very low dispersions of our PL and PW relations listed

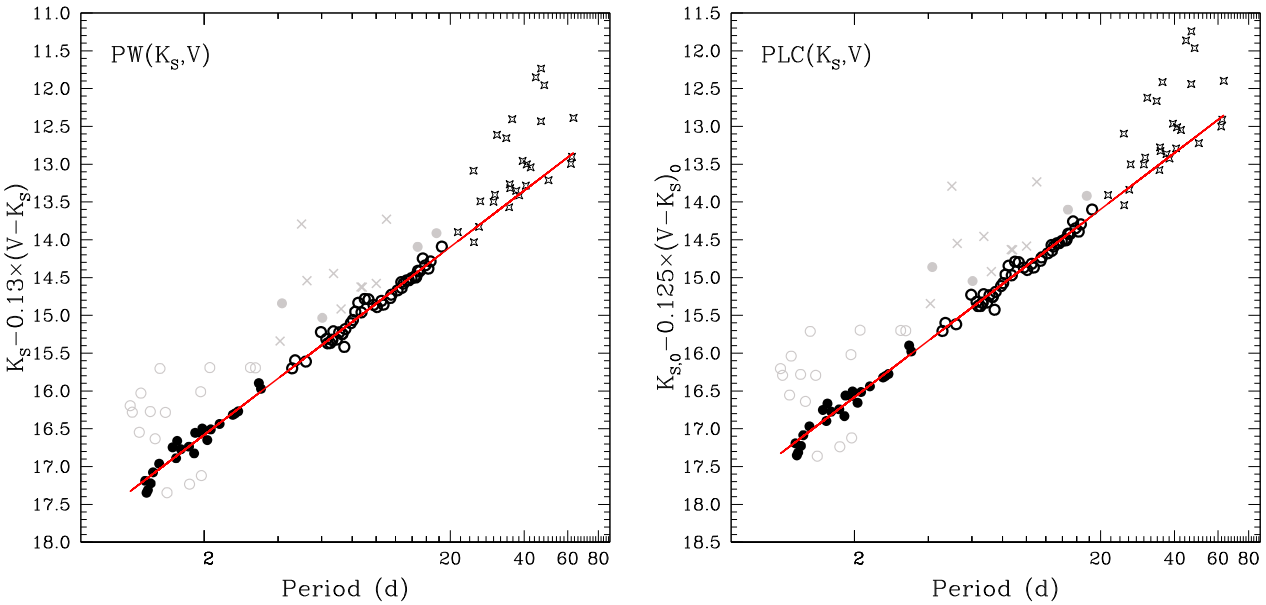

Figure 7. PW(K_s, V) and PLC(K_s, V) for the T2CEPs investigated in this paper. Symbols are as in Fig. 5.

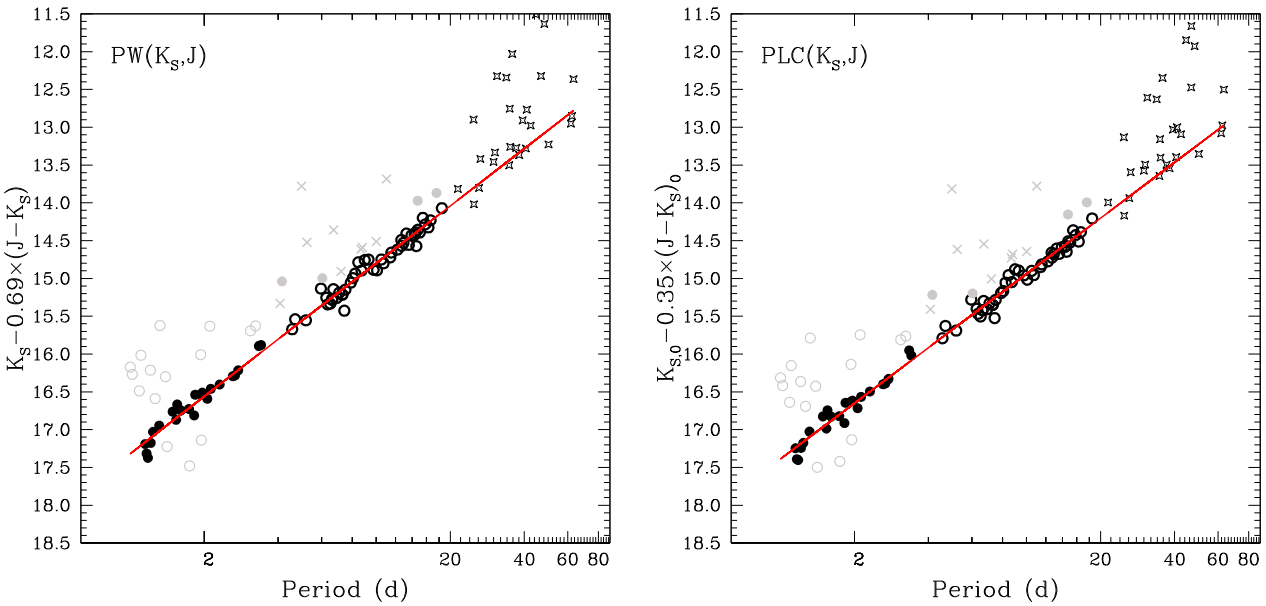

Figure 8. PW(K_s, J) and PLC(K_s, J) for the T2CEPs investigated in this paper. Symbols are as in Fig. 5.

in Table 5 seem to suggest that the metallicity dependence, if any, should be very small. Alternatively, a small dispersion in metallicity among our sample could explain the results as well. However, since the low-metallicity dependence found by Matsunaga et al. (2006) is based on T2CEPs spanning a wide range of [Fe/H], the latter explanation is less likely.

In each figure, a number of stars are shown with grey symbols. They significantly deviate from almost all relationships discussed above. The crosses represent the stars classified by Soszyński et al. (2008) as peculiar W Vir (see column 4 in Table 2), i.e. suspected binaries that do not follow the optical PL and PW relations. We note that three of these peculiar W Vir stars, namely OGLE-LMC-T2CEP-021, 052 and 083, do not show any difference with respect to the normal W Vir stars in our PL, PW and PLC planes, and were hence included in the calculations. As for BL Her and W Vir, 15 and 4 stars of the two classes were not used in the least-squares fits because, with few exceptions, they show large scattering in almost all the relationships calculated here, and, in particular in the most reliable ones, namely the PWs and PLCs based on the K_s-band photometry. The finding charts for all these stars are displayed in Fig. 2, whereas the notes in Table 2 explain in detail the causes that led us to exclude these objects, with blending by close companions being the most common cause.

Table 5 deserves some discussion: (i) the dispersion of the PL(J) relation is, as expected, larger than for the PL(K_s); (ii) for any combination of magnitude and colour, the dispersions of PW and PLC are equal (this reflects the correctness of the reddening correction applied in this paper); (iii) the PW(J, V) and PLC(J, V) are significantly more dispersed than the PW(K_s, V)–PLC(K_s, V) and PW(K_s, J)–PLC(K_s, J) couples; (iv) the best combination of

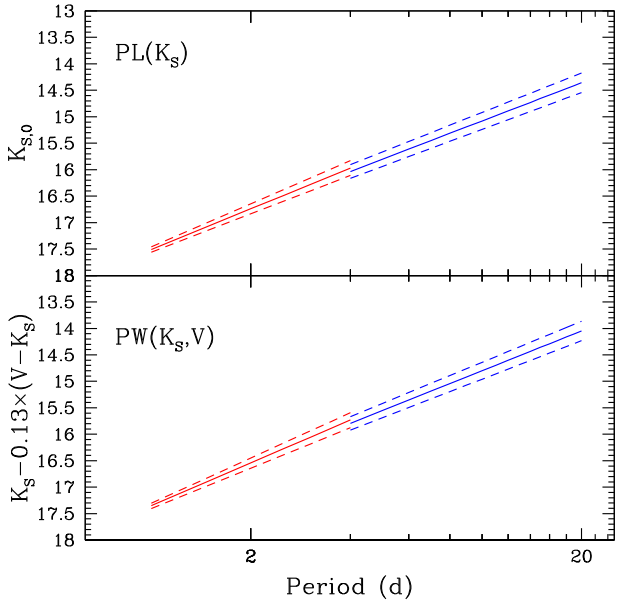

Figure 9. Top panel: PL(K_s) relation calculated separately for BL Her (red) and W Vir (blue) variables. The solid and dashed lines show the best-fits $\pm1\sigma$ error (both for slope and ZP), respectively. Bottom panel: as above but for the PW(K_s, $J - K_s$) relation.

magnitude and colour (lower dispersion) appears to be the K_s,V; (v) the colour coefficients of the PW(K_s, V) and PLC(K_s, V) relations are very similar and the two relations are coincident. Similarly, for PW(J, V) and PLC(J, V), the colour coefficients are the same within the errors, whereas this is not true for the couple PW(K_s, J) – PLC(K_s, J).

4 ABSOLUTE CALIBRATION OF PL, PLC AND PW RELATIONS

In Table 5, we provided the absolute ZP for the relevant PL, PLC and PW relations as a function of the $DM_{0,\,LMC}$. However, it is of considerable astrophysical interest to obtain an independent absolute calibration for at least some of these relations. Indeed, this would allow us to obtain an independent measure of the distance to the LMC and to the GGCs hosting T2CEP variables. To this aim, we can only rely on calibrators located close enough to the Sun to have a measurable parallax or whose distances have been estimated by Baade–Wesselink (BW) techniques (see Gautschy 1987, for a review on this method). There are only two T2CEPs whose parallaxes were measured with reasonable accuracy with the *Hubble Space Telescope* (*HST*; Benedict et al. 2011), namely κ Pav (W Vir) and VY Pyx (BL Her). For two additional BL Her variables, SW Tau and V533 Cen, as well as for κ Pav, a BW-based distance is also available (Feast et al. 2008). However, VY Pyx turned out to be a peculiar star, unusable as calibrator (see discussion in Benedict et al. 2011). As for κ Pav, the pulsational parallax estimated by Feast et al. (2008) through BW analysis is about 2σ smaller than the trigonometric parallax measured by *HST* and adopted here ($\Delta\pi = 0.67 \pm 0.33$ mas). Feast et al. (2008) investigated the possible causes of the discrepancy with respect to the *Hipparcos* parallax (van Leeuwen 2007), which was even larger than the *HST* one, but did not find any definitive explanation. A well-known potential problem related with the application of the BW technique is the uncertainty on the projection factor p (see e.g. Molinaro et al. 2012; Nardetto et al. 2014, and references therein). In their analysis, Feast et al. (2008) derived and adopted a fixed p-factor $= 1.23 \pm 0.03$. However, several researchers suggested that the p-factor actually does depend on the period of the pulsator (see e.g. Barnes 2009; Laney & Joner 2009; Storm et al. 2011a; Nardetto et al. 2014, and references therein); hence, for example, different p-factor values should be used for BL Her and W Wir stars. Given the uncertainties on the projection factor discussed above, in the following, we will adopt the *HST*-based distance for κ Pav, and the ZP of the different PL, PW and PLC relations will be estimated including or not the BW-based distances for SW Tau and V533 Cen. Finally, we note that [Fe/H](κ Pav) $\approx +0.0$ dex (Feast et al. 2008), i.e. at least 1 dex more metal rich than expected for typical T2CEPs. Hence, some additional uncertainty when using this object as a distance indicator can be caused by a possible metallicity effect. However, as discussed in Section 3, the metal dependence of the T2CEP PLs, if any, should be very small, and we do not expect the high metallicity of κ Pav to be an issue for our purposes. To enlarge the number of reliable calibrators, a possibility is to use the five RR Lyrae stars whose parallaxes were measured with *HST* by Benedict et al. (2011). Indeed, as already hypothesized by Sollima, Cacciari & Valenti (2006) and Feast et al. (2008), RR Lyrae and T2CEPs follow the same PL(K_s) relation (Caputo et al. 2004 found similar results in the optical bands). To further test this possibility, we draw in Fig. 10 the PL(K_s) and PW(K_s) relations for the T2CEPs analysed in this paper, in comparison with the location occupied in the same planes by the RR Lyrae stars in the LMC (light blue filled circles, after Borissova et al. 2009). The periods of c-type RR Lyrae stars were fundamentalized by adding $\delta \log P = 0.127$ (Bono et al. 1997a) and the magnitudes have been corrected for the metallicity term devised by Sollima et al. (2006), using the individual metallicity measurement compiled by Borissova et al. (2009). It can be seen that both the PL(K_s) and PW(K_s) relations (red lines) derived for T2CEPs in Section 5 tightly match the location of the RR Lyrae stars. On this basis, we decided to proceed using also the RR Lyrae with *HST* parallax to anchor the ZP of the PL(K_s) and PW(K_s, V) relations for T2CEPs. To this aim, we simply adopted the slopes of

Table 5. Relevant relationships derived in this work. Note that all the results are in the VISTA photometric system. $DM_{0,\,LMC}$ stands for the LMC dereddened DM.

Method	Relation	rms (mag)
PL(J)	$M_{J,0} = (-2.19 \pm 0.04)\log P + (17.700 \pm 0.035) - DM_{0,\,LMC}$	0.13
PL(K_s)	$M_{K_{s,0}} = (-2.385 \pm 0.03)\log P + (17.47 \pm 0.02) - DM_{0,\,LMC}$	0.09
PW(J, V)	$M_J - 0.41(V - J) = (-2.290 \pm 0.035)\log P + (17.19 \pm 0.03) - DM_{0,\,LMC}$	0.11
PLC(J, V)	$M_{J,0} = (-2.40 \pm 0.05)\log P + (0.35 \pm 0.07)(V - J)_0 + (17.385 \pm 0.065) - DM_{0,\,LMC}$	0.11
PW(K_s, V)	$M_{K_s} - 0.13(V - K_s) = (-2.49 \pm 0.03)\log P + (17.33 \pm 0.02) - DM_{0,\,LMC}$	0.08
PLC(K_s, V)	$M_{K_{s,0}} = (-2.48 \pm 0.04)\log P + (0.125 \pm 0.040)(V - K_s)_0 + (17.33 \pm 0.05) - DM_{0,\,LMC}$	0.08
PW(K_s, J)	$M_{K_s} - 0.69(J - K_s) = (-2.52 \pm 0.03)\log P + (17.320 \pm 0.025) - DM_{0,\,LMC}$	0.085
PLC(K_s, J)	$M_{K_{s,0}} = (-2.45 \pm 0.04)\log P + (0.35 \pm 0.14)(J - K_s)_0 + (17.39 \pm 0.04) - DM_{0,\,LMC}$	0.085

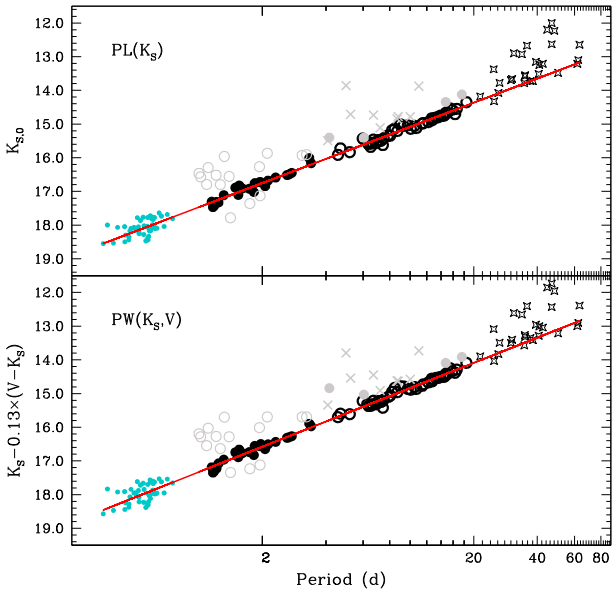

Figure 10. PL(K_s) and PW(K_s, V) relations for the T2CEPs analysed in this paper (symbols as in Fig. 5) and for the sample of RR Lyrae stars in the LMC observed by Borissova et al. (2009, light blue filled circles). The red lines show the relationships listed in Table 5 extended till the periods of the RR Lyrae stars.

the quoted relations from Table 5, corrected for metallicity the ZP for the five RR Lyrae stars with *HST* parallaxes and calculated the weighted average of the results in two cases: (i) including only stars with *HST* parallax, namely, κ Pav and the five RR Lyrae stars; (ii) using the stars at point (i) plus the two T2CEPs with BW analysis, namely SW Tau and V533 Cen.[8] The results of these procedures are outlined in Table 6 (columns 3 and 4) and in Fig. 11. For comparison, column (2) of Table 6 shows the ZPs obtained assuming $DM_{0,\,LMC} = 18.46 \pm 0.03$ mag, as derived by Ripepi et al. (2012b) from LMC CC stars. We choose the work by Ripepi et al. (2012b) as reference for CCs because (i) these authors adopted a procedure similar to the one adopted in this work; (ii) their results are in excellent agreement with the most recent and accurate literature findings (see e.g. Storm et al. 2011b; Joner & Laney 2012; Laney et al. 2012; Walker 2012; Pietrzyński et al. 2013; de Grijs et al. 2014, and references therein). An analysis of Table 6 reveals that (i) the inclusion of the two stars with BW-based distances does not change significantly the ZPs and (ii) there is a difference of at least ∼0.1 mag between the ZPs calibrated on the basis of CCs and of Galactic T2CEPs (see Section 5).

4.1 Comparison with the literature

The relationships presented in Tables 5 and 6 can now be compared to those available in the literature. As mentioned in the introduction, Matsunaga et al. (2006, 2009) published the PL relations in the JHK_s bands for BL Her and W Vir variables hosted by GGCs and the LMC, respectively. These results can be compared with ours, provided that we first transform all the J and K_s magnitudes into the VISTA system. With this aim, we transformed the Matsunaga et al. (2006) photometry from 2MASS to VISTA using the equations reported in Section 2.1. The results of Matsunaga et al. (2009) are in the IRSF system, whose J and K_s can in principle be transformed to the 2MASS system (Kato et al. 2007), and in turn, into the VISTA system. However, this is not possible for the J band, because we lack H-band photometry (see table 10 in Kato et al. 2007). We can safely overcome this problem by noting that the $(J - H)$ colour for BL Her and W Vir stars spans a very narrow range ($0.25 < (J - H) < 0.4$ mag; see e.g. Matsunaga et al. 2011) so that, according to Kato et al. (2007), we can assume $J(\mathrm{IRSF}) = J(\mathrm{2MASS}) + (0.005 \pm 0.005)$. Finally, since our targets span the range $0.25 < (J - K_s) < 0.6$ mag, we obtained $J(\mathrm{IRSF}) = J(\mathrm{VISTA}) + (0.035 \pm 0.015)$. As for the K_s, the transformation is straightforward: $K_s(\mathrm{IRSF}) = K_s(\mathrm{VISTA}) + (0.014 \pm 0.001)$.

The PL relations by Matsunaga et al. (2006, 2009), corrected as discussed above, are presented in the first four rows of Table 7. We can compare directly the PL(J) and PL(K_s) relations for the LMC (lines 2 and 4 in Table 7) with our results (lines 1 and 2 in Table 5). There is very good agreement within 1σ errors for the PL(J), whereas for the PL(K_s), the comparison is slightly worse, especially concerning the slope of the relation which is discrepant at the 1.5σ level. It is also worth mentioning that the dispersion of our relations is significantly smaller, as a result of the much better light-curve sampling of the VMC data.

As for the PL(J) and PL(K_s) derived for GGCs by Matsunaga et al. (2006), their slopes are in very good agreement with ours, which suggest a 'universal slope' in the NIR filters, independent of the galactic environment. As for the ZPs, we can only compare them for the PL(K_s) relations (see Table 6). We found excellent agreement when the ZP is calibrated through the Galactic calibrators (irrespectively of whether stars with BW measures are included or not), whereas there is a 0.12 mag discrepancy if the ZP is calibrated by means of the LMC DM coming from CCs. This occurrence is not surprising, since Matsunaga et al. (2006) used the M_V versus [Fe/H] relation for RR Lyrae variables by Gratton et al. (2003) to estimate the distances of the GGCs hosting T2CEPs and derive their PL(K_s). Hence, the two Population II calibrators, RR Lyrae and T2CEPs, give distance scales in agreement with each other.

A similar comparison can be performed with the theoretical predictions by Di Criscienzo et al. (2007), who in addition calculated the PWs for all the combinations of magnitudes and colours of interest in this work. Again, we converted the Di Criscienzo et al. (2007) results from Bessell & Brett (1988, BB) to the VISTA system. To do this, we used the transformations BB-2MASS from Carpenter (2001) and 2MASS-VISTA (see Section 2.1) and the same procedure as above to derive $J(\mathrm{BB}) = J(\mathrm{VISTA}) + (0.04 \pm 0.010)$ and $K_s(\mathrm{BB}) = K_s(\mathrm{VISTA}) + (0.030 \pm 0.015)$. Secondly, since the predicted PL and PW relations mildly depend on metallicity and adopted a mixing length parameter (α[9]), we have to make a choice for these parameters. We decided to evaluate the relations for $\alpha = 1.5 \pm 0.5$ (to encompass reasonable values for α) and [Fe/H] $= -1.5 \pm 0.3$ dex as an average value for the LMC old population (see e.g. Borissova et al. 2004, 2006; Gratton et al. 2004; Haschke et al. 2012). The uncertainties on these parameters were taken into account in re-deriving the ZP of the predicted PL and PW relations in the VISTA system. The result of this procedure is shown in the second part of Table 7. A comparison with

[8] The uncertainties on the DM of these two objects were obtained by summing the uncertainties reported in table 4 of Feast et al. (2008).

[9] $\alpha = l/H_p$ is the ratio between the mean free path of a convective element (l) and the pressure scale height (H_p). Varying this parameter strongly affects the properties of a star's outer envelope such as its radius and effective temperature.

Table 6. PL(K_s) and PW(K_s) relations for LMC T2CEPs with the ZP calibrated as follows: (2) by imposing a $DM_{0,LMC} = 18.46 \pm 0.03$ mag (from CCs in the LMC; Ripepi et al. 2012b) in Table 5; (3) by adopting Galactic T2CEP (κ Pav) and RR Lyrae variables with *HST* parallaxes (Benedict et al. 2011) and T2CEPs with BW distance estimates (Feast et al. 2008); (4) by adopting only calibrators with the quoted *HST* parallaxes. See the text for additional details.

Relation (1)	ZP_{CC} (2)	$ZP_{\pi+BW}$ (3)	ZP_{π} (4)
$K_{s,0} = (-2.385 \pm 0.03)\log P + ZP$	-0.99 ± 0.04	-1.09 ± 0.10	-1.11 ± 0.10
$K_s - 0.13(V-K_s) = (-2.49 \pm 0.03)\log P + ZP$	-1.13 ± 0.04	-1.24 ± 0.10	-1.26 ± 0.10

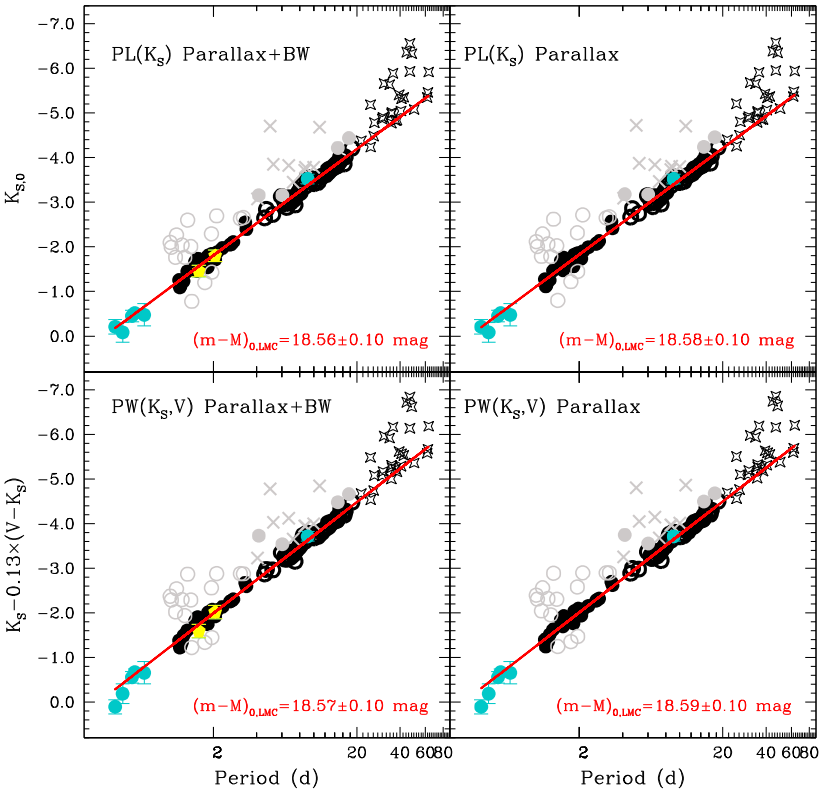

Figure 11. Absolute PL(K_s) and PW(K_s, V) relations for the T2CEPs analysed in this paper (symbols as in Fig. 5). Light blue and yellow filled circles show the objects whose distances were measured through *HST* parallaxes (Benedict et al. 2011) or through BW analysis (Feast et al. 2008), respectively. The red line shows the best-fitting line to the data adopting the slope from Table 5, while ZP*s* were calculated using the objects with *HST* parallaxes alone (right-hand panels), and by adding to them the objects with BW analysis (left-hand panels). The true DMs estimated in each case for the LMC are also labelled (see Section 5).

Table 6 shows that both for the PL(K_s) and PW(K_s, V) relations, there is excellent agreement between ours and theoretical results if the quoted relationships are calibrated with the Galactic T2CEPs and RR Lyrae, whereas there is an ∼0.1 mag discrepancy if we adopt the CC-based DM by Ripepi et al. (2012b) for the LMC to define the ZP. However, if we take into account the uncertainties, this discrepancy results formally not significant within 1σ.

5 DISCUSSION

The results reported in Section 4 allow us to discuss the distance of the LMC as estimated from NIR observation of the T2CEPs hosted in this galaxy. Table 8 (columns 3 and 4) lists the $DM_{0,LMC}$ calculated using the different ZP estimates for the PL(K_s) and PW(K_s, V) relations listed in Table 6. An inspection of the table reveals that the $DM_{0,LMC}$ calculated by means of CCs (column 2 in Table 8) and by means of the T2CEPs differ by more than ∼0.1 mag, even if, formally, there is agreement within 1σ. Since both the Ripepi et al. (2012b) calibration for CCs and that presented here for T2CEPs are based on a weighted mix of *HST* parallaxes and BW analysis, this discrepancy, albeit only partially significant, seems to suggest that the distance scales calibrated on pulsating stars belonging to Population I and Population II give different results (for a recent comprehensive review of the literature and a discussion about this argument, see de Grijs et al. 2014).

An additional application of the absolute PL(K_s) relation for T2CEPs concerns the distance estimate of GGCs hosting such kind of pulsators. Homogeneous K_s photometry, as well as period of pulsation for most of the known T2CEPs in GGCs, was published by Matsunaga et al. (2006, see their table 2). We simply inserted the period of these variables in the PL(K_s) of Table 6, and by difference with the observed magnitudes, we derived the DM for each GGC. When more than one T2CEP was present in a cluster, we averaged the resulting DMs (we excluded from the calculations the variables

Table 7. Values for the coefficients of the PL, PW and PLC relations for BL Her and W Vir Cepheids taken from the literature. The PW functions are defined as in Table 5. The errors of ZP take into account the uncertainties in the transformation of the J and K_s photometry to the VISTA system (see the text for details).

Method	Relation	σ (mag)
Results by Matsunaga et al. (2006, 2009) transformed to the VISTA system		
PL(J) GCs	$M_{J,0} = (-2.23 \pm 0.05)\log P - (0.84 \pm 0.03)$	0.16
PL(J) LMC	$J_0 = (-2.16 \pm 0.04)\log P + (17.76 \pm 0.03)$	0.21
PL(K_s) GCs	$M_{K_{s,0}} = (-2.41 \pm 0.05)\log P - (1.11 \pm 0.03)$	0.14
PL(K_s) LMC	$K_{s,0} = (-2.28 \pm 0.05)\log P + (17.40 \pm 0.03)$	0.21
Results by Di Criscienzo et al. (2007) transformed to the VISTA system		
PL(J)	$M_{J,0} = (-2.29 \pm 0.04)\log P - (0.73 \pm 0.13)$	
PL(K_s)	$M_{K_{s,0}} = (-2.38 \pm 0.02)\log P - (1.10 \pm 0.07)$	
PW(J, V)	$M_J - 0.41(V-J) = (-2.37 \pm 0.02)\log P - (1.15 \pm 0.08)$	
PW(K_s, V)	$M_{K_s} - 0.13(V-K_s) = (-2.52 \pm 0.02)\log P - (1.25 \pm 0.08)$	
PW(K_s, J)	$K_s - 0.69(J-K_s) = (-2.60 \pm 0.02)\log P - (1.27 \pm 0.08)$	

Table 8. DM of the LMC estimated on the basis of the different PL(K_s) and PW(K_s) relations described in Table 6 (see the text).

Relation (1)	DM_{CC}^{LMC} (2)	$DM_{\pi+BW}^{LMC}$ (3)	DM_{π}^{LMC} (4)
PL(K_s)	18.46 ± 0.04	18.56 ± 0.10	18.58 ± 0.10
PW(K_s, V)	18.46 ± 0.04	18.57 ± 0.10	18.59 ± 0.10

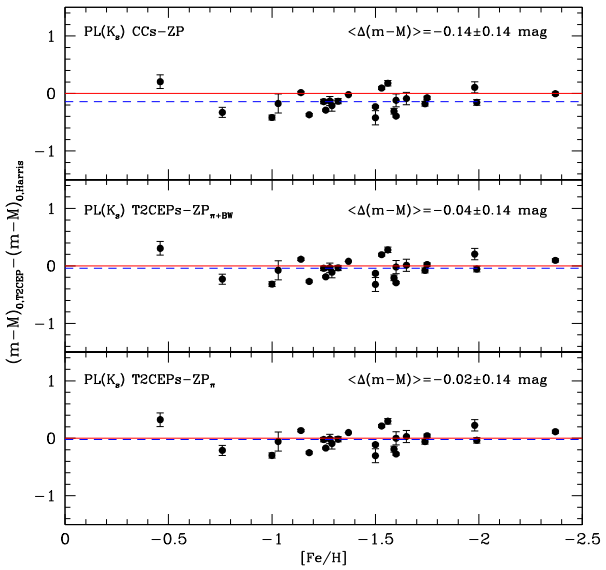

Figure 12. DM differences (this work−Harris 1996) for a sample of GGCs hosting T2CEPs as a function of [Fe/H]. The dashed blue line shows the average difference. The solid red line shows the line with zero difference. The DMs for the GGCs were estimated adopting the PL(K_s) for T2CEPs and ZP determined as follows: (top panel) on the basis of the $DM_{0,LMC}$ measured by Ripepi et al. (2012b) using LMC CC with VMC NIR data; (middle panel) by means of a sample of Galactic T2CEPs whose distances were measured both through *HST* parallaxes (Benedict et al. 2011) and BW technique (Feast et al. 2008); (bottom panel) as in the previous case, but using objects with *HST* parallaxes only.

with periods longer than about 35 d because they are likely neither BL Her nor W Vir variables). The result of such a procedure is shown in Fig. 12 where for each GGC analysed here, we show (as a function of the metal content of the clusters) the difference between the DMs estimated on the basis of the three different calibration of the PL(K_s) listed in Table 6 and the DMs reported by Harris (1996) in his catalogue of GGC parameters. In Fig. 12, the average discrepancy in DMs decreases from top to bottom, suggesting that, even if the statistical significance is low (due to the large dispersion in ΔDM values ~ 0.14 mag), the distance scale of GGCs, if estimated on the basis of the T2CEPs hosted in this system, is more consistent with Population II rather than Population I standard candles. This is not particularly surprising since most of the distances of GGCs in the Harris catalogue are based on RR Lyrae stars.

6 SUMMARY

In the context of the VMC survey, this paper shows the first results concerning T2CEPs in the LMC. We presented J and K_s light curves for 130 pulsators, including 41 BL Her, 62 W Vir (12 pW Vir) and 27 RV Tau variables, corresponding to 63, 63 (75 per cent) and 61 per cent of the known LMC populations of the three variable classes, respectively. The K_s-band light curves are almost always well sampled, allowing us to obtain accurate spline fits to the data and, in turn, precise intensity-averaged $\langle K_s \rangle$ magnitudes for 120 variables in our sample. As for the J band, only about 1/3 of the J light curves were sufficiently sampled to allow a satisfactory spline fit to the data, and for the remaining 2/3 of pulsators, the intensity-averaged $\langle J \rangle$ magnitudes were derived using the K_s-band spline fits as templates. On the basis of this data set for BL Her and W Vir, complemented by the $\langle V \rangle$ magnitudes from the OGLE survey, we have built for the first time (apart from PL(J) and PL(K_s)) a variety of empirical PL, PLC and PW relationships, for any combination of the V, J, K_s filters. Several outliers were removed from the calculation of these relations, and we provided an explanation for the presence of these divergent objects. All the quoted PL, PLC and PW relationships were calibrated in terms of the LMC distance. However, the availability of absolute M_V and M_{K_s} for a small sample of RR Lyrae and T2CEPs variables based on *HST* parallaxes allowed us to obtain an independent absolute calibration of the PL(K_s) and PW(K_s, V) relationships [the PLC(K_s, V) is identical to the PW(K_s, V)]. If applied to the LMC and to the GGCs hosting T2CEPs, these relations give DMs which are around 0.1 mag longer than those estimated for CCs by means of *HST* parallaxes and BW techniques. However, if we take into account the uncertainties at their face value, the quoted discrepancy is formally not significant within 1σ.

ACKNOWLEDGEMENTS

We wish to thank our referee, Dr C. D. Laney, for his helpful and competent review of the manuscript. VR warmly thanks Roberto Molinaro for providing the program for the spline interpolation of the light curves.

Partial financial support for this work was provided by PRIN-INAF 2011 (PI: Marcella Marconi) and PRIN MIUR 2011 (PI: F. Matteucci). We thank the UK's VISTA Data Flow System comprising the VISTA pipeline at the Cambridge Astronomy Survey Unit (CASU) and the VISTA Science Archive at Wide Field Astronomy Unit (Edinburgh) (WFAU) for providing calibrated data products supported by the STFC. This work was partially supported by the Gaia Research for European Astronomy Training (GREAT-ITN) Marie Curie network, funded through the European Union Seventh Framework Programme ([FP7/2007- 1312 2013] under grant agreement no. 264895). RdG acknowledges research support from the National Natural Science Foundation of China (NSFC) through grant 11373010. This work was partially supported by the Argentinian institutions CONICET and Agencia Nacional de Promoción Científica y Tecnológica (ANPCyT).

REFERENCES

Barnes T. G., 2009, in Guzik J. A., Bradley P. A., eds, AIP Conf. Proc. Vol. 1170, Stellar Pulsation: Challenges for Theory and Observation. Am. Inst. Phys., New York, p. 3
Bekki K., Chiba M., 2007, MNRAS, 381, L16
Benedict G. F. et al., 2011, AJ, 142, 187
Bessell M. S., Brett J. M., 1988, PASP, 100, 1134
Bono G., Caputo F., Castellani V., Marconi M., 1997a, A&AS, 121, 327
Bono G., Caputo F., Santolamazza P., 1997b, A&A, 317, 171
Borissova J., Minniti D., Rejkuba M., Alves D., Cook K. H., Freeman K. C., 2004, A&A, 423, 97
Borissova J., Minniti D., Rejkuba M., Alves D., 2006, A&A, 460, 459
Borissova J., Rejkuba M., Minniti D., Catelan M., Ivanov V. D., 2009, A&A, 502, 505
Brocato E., Caputo F., Castellani V., Marconi M., Musella I., 2004, AJ, 128, 1597
Caputo F., 1998, A&AR, 9, 33
Caputo F., Castellani V., Degl'Innocenti S., Fiorentino G., Marconi M., 2004, A&A, 424, 927
Cardelli J. A., Clayton G. C., Mathis J. S., 1989, ApJ, 345, 245
Carpenter J. M., 2001, AJ, 121, 2851
Cioni M.-R. L., Clementini G., Girardi L. et al., 2011, A&A, 527, 116
Clementini G., Gratton R., Bragaglia A., Carretta E., Di Fabrizio L., Maio M., 2003, AJ, 125, 1309
Cross N. J. G. et al., 2012, A&A, 548, A119
Dalton G. B. et al., 2006, in McLean I. S., Iye M., eds, Proc. SPIE Conf. Ser. Vol. 6269, Ground-Based and Airborne Instrumentation for Astronomy. SPIE, Bellingham, p. 62690X
de Grijs R., Wicker J. E., Bono G., 2014, AJ, 147, 122
Di Criscienzo M., Caputo F., Marconi M., Cassisi S., 2007, A&A, 471, 893
Emerson J. P. et al., 2004, SPIE, 5493, 401
Emerson J. P., McPherson A., Sutherland W., 2006, The Messenger, 126, 41
Feast M. W., 2010, in Proc. Int. Conf., Variable Stars, the Galactic halo and Galaxy Formation. Sternberg Astronomical Institute of Moscow University, Russia, p. 45
Feast M. W., Laney C. D., Kinman T. D., van Leeuwen F., Whitelock P. A., 2008, MNRAS, 386, 2115
For B.-Q., Staveley-Smith L., McClure-Griffiths N. M., 2013, ApJ, 764, 74
Freedman W. L. et al., 2001, ApJ, 553, 47
Gao J., Jiang B. W., Li A., Xue M. Y., 2013, ApJ, 776, 7
Gautschy A., 1987, Vistas Astron., 30, 197
Gingold R. A., 1985, Mem. Soc. Astron. Ital., 56, 169
Gratton R. G., Bragaglia A., Carretta E., Clementini G., Desidera S., Grundahl F., Lucatello S., 2003, A&A, 408, 529
Gratton R. G., Bragaglia A., Clementini G., Carretta E., Di Fabrizio L., Maio M., Taribello E., 2004, A&A, 421, 937
Groenewegen M. A. T., Udalski A., Bono G., 2008, A&A, 481, 441
Harris H. C., 1985, AJ, 90, 756
Harris W. E., 1996, AJ, 112, 1487
Harris J., Zaritsky D., 2004, AJ, 127, 1531
Harris J., Zaritsky D., 2009, AJ, 138, 1243
Haschke R., Grebel E. K., Duffau S., 2011, AJ, 141, 158
Haschke R., Grebel E. K., Duffau S., Jin S., 2012, AJ, 143, 48
Irwin M. J., 2009, UKIRT Newsl., 25, 15
Irwin M. J. et al., 2004, Proc. SPIE, 5493, 411
Joner M. D., Laney C. D., 2012, AAS/Division of Dynamical Astronomy Meeting, 43, #09.02
Kato D. et al., 2007, PASJ, 59, 615
Kubiak M., Udalski A., 2003, Acta Astron., 53, 117
Laney C. D., Joner M. D., 2009, in Guzik J. A., Bradley P. A., eds, AIP Conf. Proc. Vol. 1170, Stellar Pulsation: Challenges for Theory and Observation. Am. Inst. Phys., New York, p. 93
Laney C. D., Joner M. D., Pietrzyński G., 2012, MNRAS, 419, 1637
Madore B. F., 1982, ApJ, 253, 575
Madore B. F., Freedman W., 1991, PASP, 103, 933
Madore B. F., Freedman W. L., 2012, ApJ, 744, 132
Marconi M., Di Criscienzo M., 2007, A&A, 467, 223
Matsunaga N. et al., 2006, MNRAS, 370, 1979
Matsunaga N., Feast M. W., Menzies J. W., 2009, MNRAS, 397, 933
Matsunaga N., Feast M. W., Soszyński I., 2011, MNRAS, 413, 223
Matteucci A., Ripepi V., Brocato E., Castellani V., 2002, A&A, 387, 861
Molinaro R. et al., 2012, ApJ, 748, 69
Moretti M. I., Clementini G., Muraveva T. et al., 2014MNRAS, 437, 2702
Muller E., Stanimirović S., Rosolowsky E., Staveley-Smith L., 2004, ApJ, 616, 845
Nardetto N., Storm J., Gieren W., Pietrzyński G., Poretti E., 2014, in Guzik J. A., Chaplin W. J., Handler G., Pigulski A., eds, Proc. IAU Symp. 301, Precision Asteroseismology. Cambridge Univ. Press, Cambridge, p. 145
Neilson H. R., Langer N., 2012, A&A, 537, 26
Nemec J. M., Nemec A. F. L., Lutz T. E., 1994, AJ, 108, 222
Pietrzyński G. et al., 2013, Nature, 495, 76
Pritzl B. J., Smith H. A., Stetson P. B., Catelan M., Sweigart A. V., Layden A. C., Rich R. M., 2003, AJ, 126, 1381
Putman M. E. et al., 1998, Nature, 394, 752
Riess A. et al., 2011, ApJ, 730, 119
Ripepi V., Moretti M. I., Clementini G., Marconi M., Cioni M.-R. L., Marquette J. B., Tisserand P., 2012a, Ap&SS, 341, 51
Ripepi V. et al., 2012b, MNRAS, 424, 1807
Ripepi V. et al., 2014a, MNRAS, 437, 2307
Ripepi V. et al., 2014b, MNRAS, 442, 1897
Rubele S. et al., 2012, A&A, 537, A106
Sandage A., Tammann G. A., 2006, ARA&A, 44, 93
Skrutskie M. F. et al., 2006, AJ, 131, 1163
Sollima A., Cacciari C., Valenti E., 2006, MNRAS, 372, 1675
Soszyński I. et al., 2008, Acta Astron., 58, 293
Soszyński I. et al., 2012, Acta Astron., 62, 219
Stanimirović S., Staveley-Smith L., Jones P. A., 2004, ApJ, 604, 176
Storm J. et al., 2011a, A&A, 534, A94
Storm J., Gieren W., Fouqué P., Barnes T. G., Soszyński I., Pietrzyński G., Nardetto N., Queloz D., 2011b, A&A, 534, A95
Subramanian S., Subramaniam A., 2013, A&A, 552, A144
Udalski A., Szymanski M., Kaluzny J., Kubiak M., Mateo M., 1992, Acta Astron., 42, 253
van der Marel R. P., Cioni M.-R. L., 2001, AJ, 122, 1807
van Leeuwen F., 2007, Astrophysics and Space Science Library, Vol. 350, Hipparcos, the New Reduction of the Raw Data. Springer, Berlin
Venzmer M. S., Kerp J., Kalberla P. M. W., 2012, A&A, 547, A12
Walker A., 2012, Ap&SS, 341, 43
Wallerstein G., 2002, PASP, 114, 689
Wallerstein G., Cox A. N., 1984, PASP, 96, 677

APPENDIX A: LIGHT CURVES

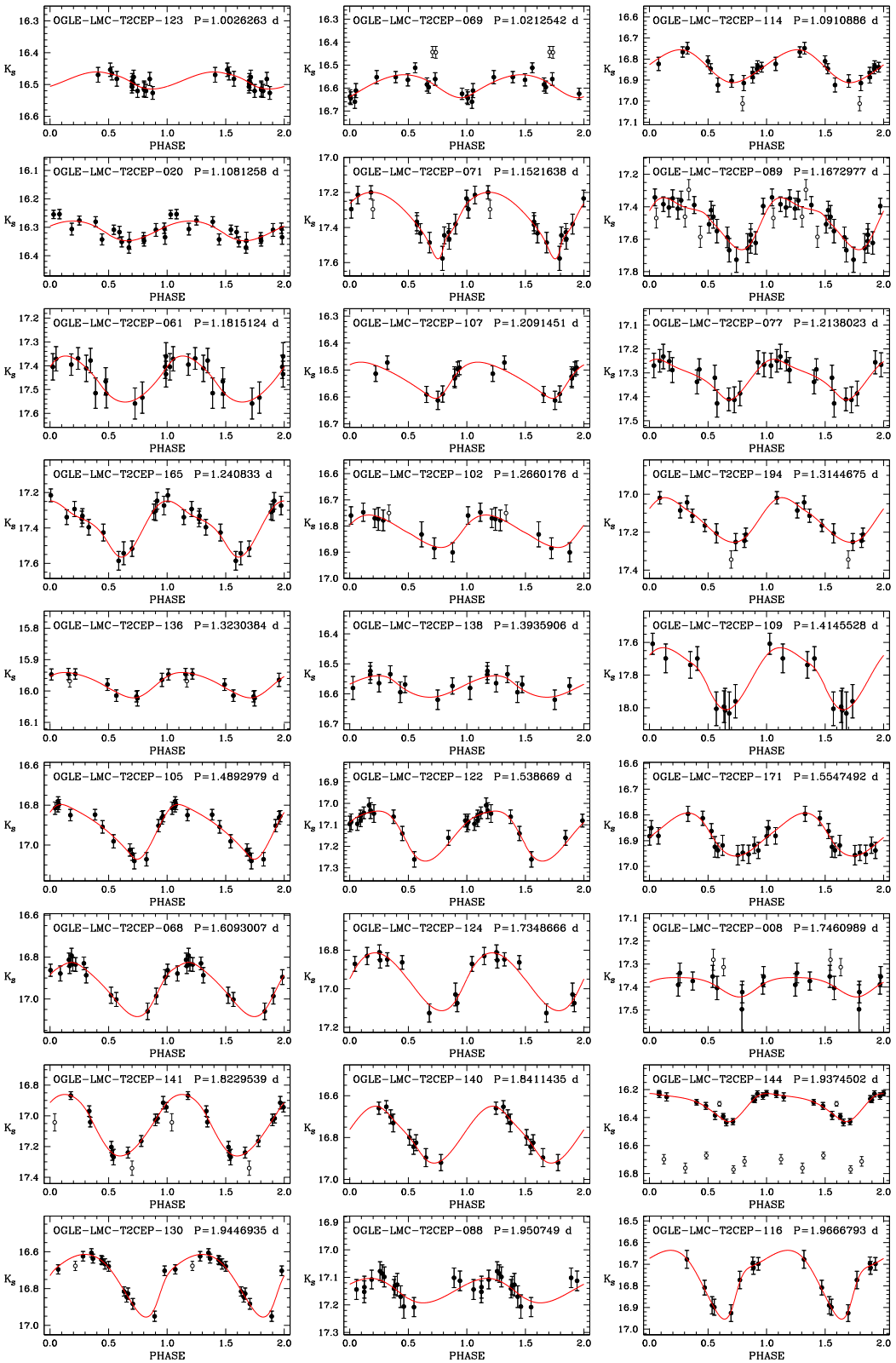

Figure A1. K_s-band light curves for T2CEPs with usable data discussed in this paper. Stars are displayed in order of increasing period. Filled and open circles represent phase points used or not used in the fitting procedure, respectively. Solid lines represent best-fitting splines to the data (see the text). In each panel, we report OGLE's identification number and period.

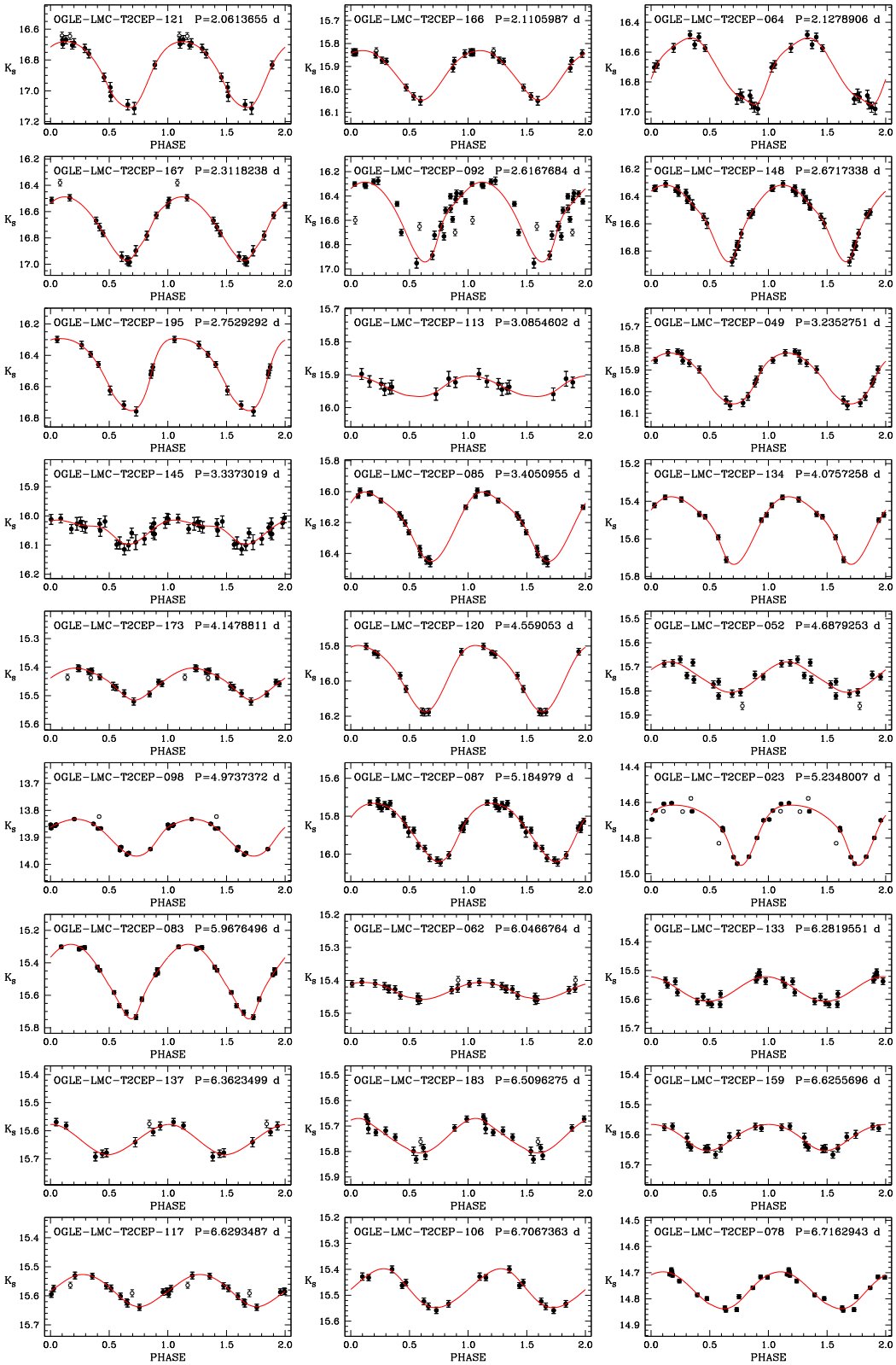

Figure A1 – *continued*

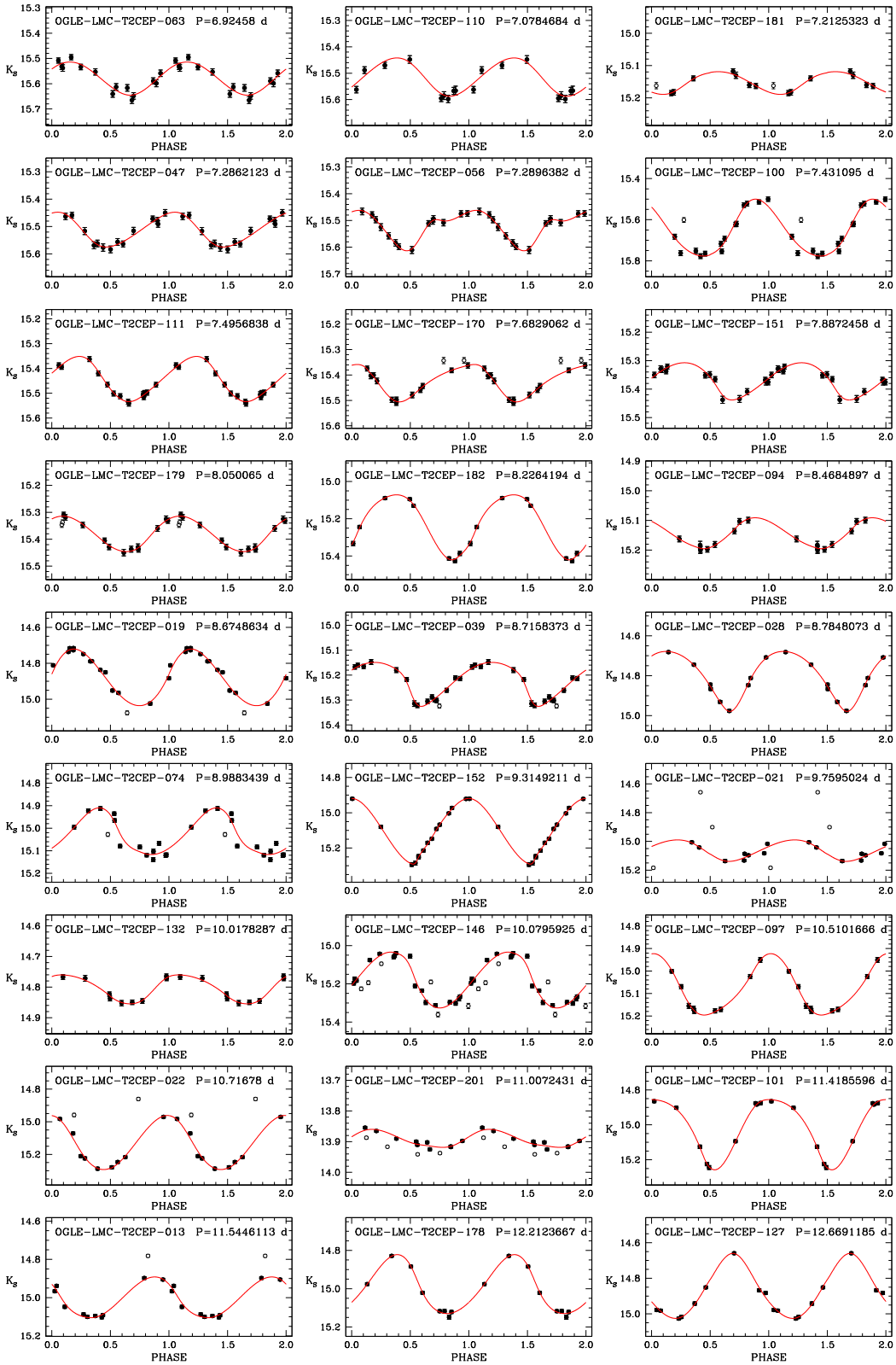

Figure A1 – *continued*

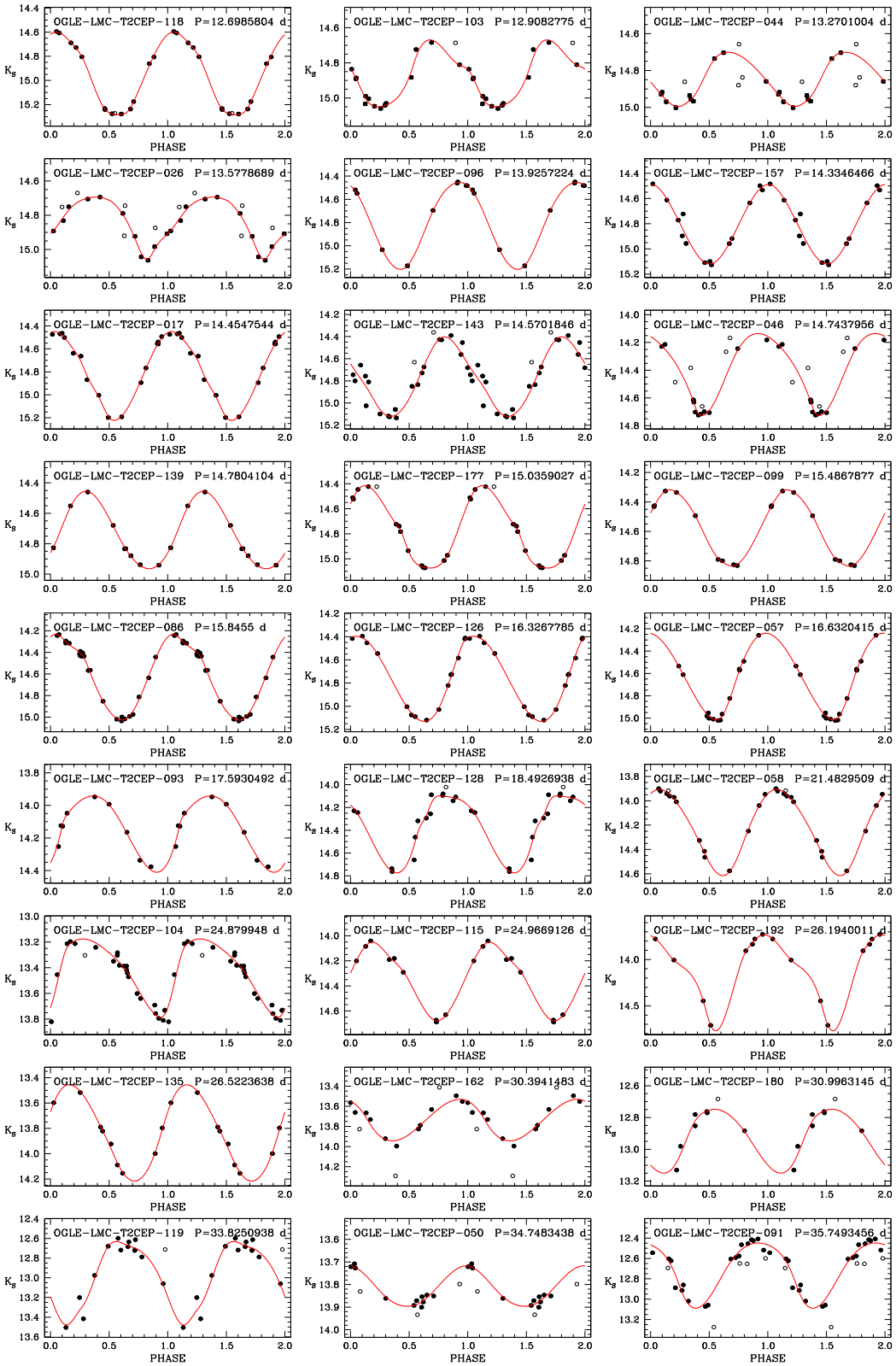

Figure A1 – *continued*

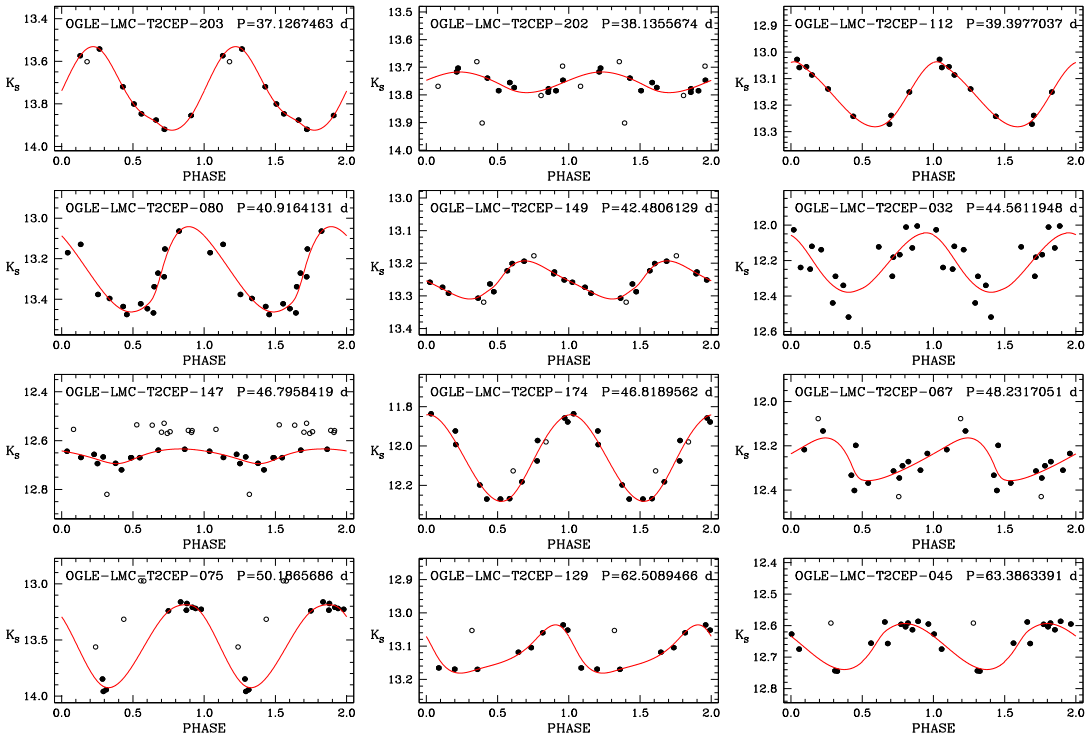

Figure A1 – *continued*

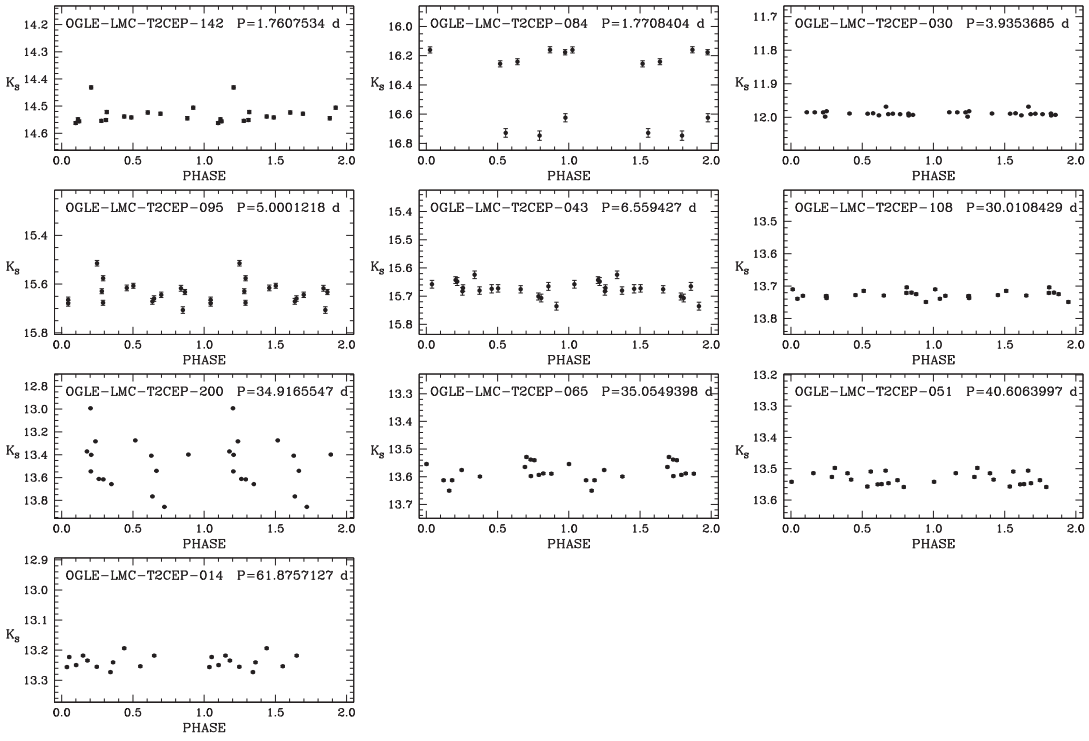

Figure A2. K_s-band light curves for problematic stars (see the text).

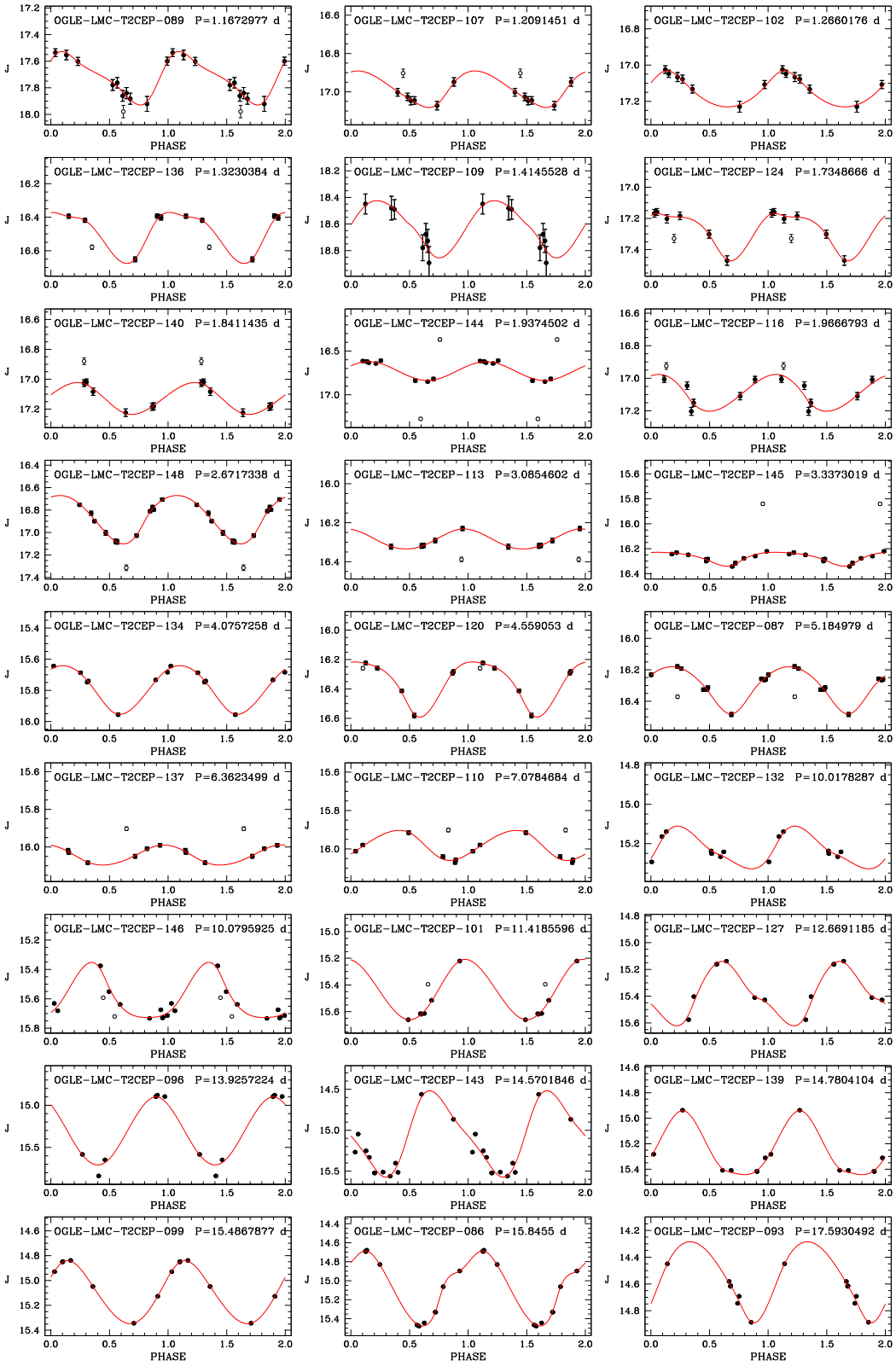

Figure A3. *J*-band light curves for T2CEP stars with a sufficient number of epochs to perform the spline fit to the data. Stars are displayed in order of increasing period. Solid lines represent spline best fits to the data (see the text). In each panel, we report OGLE's identification number and period.

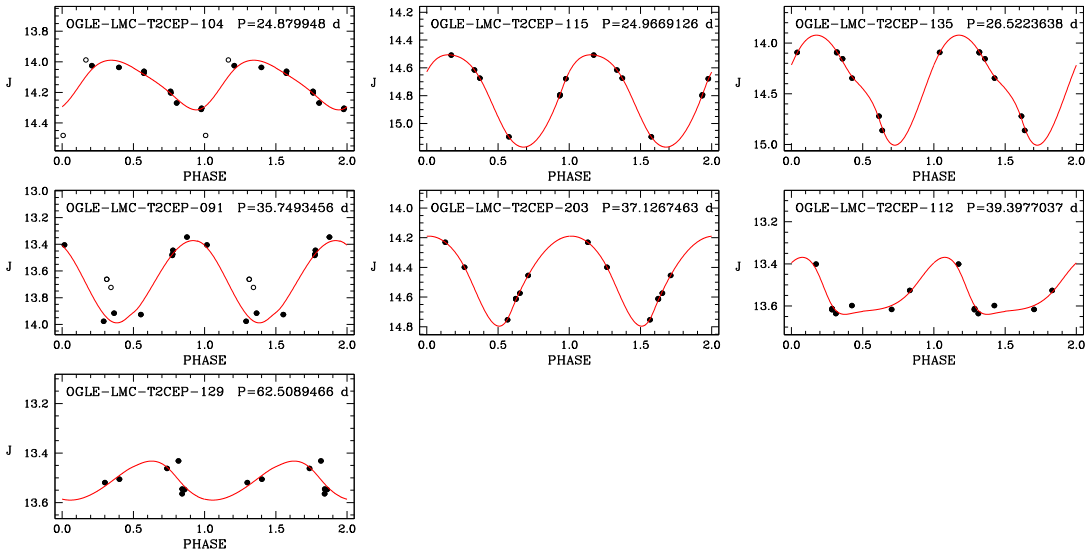

Figure A3 – *continued*

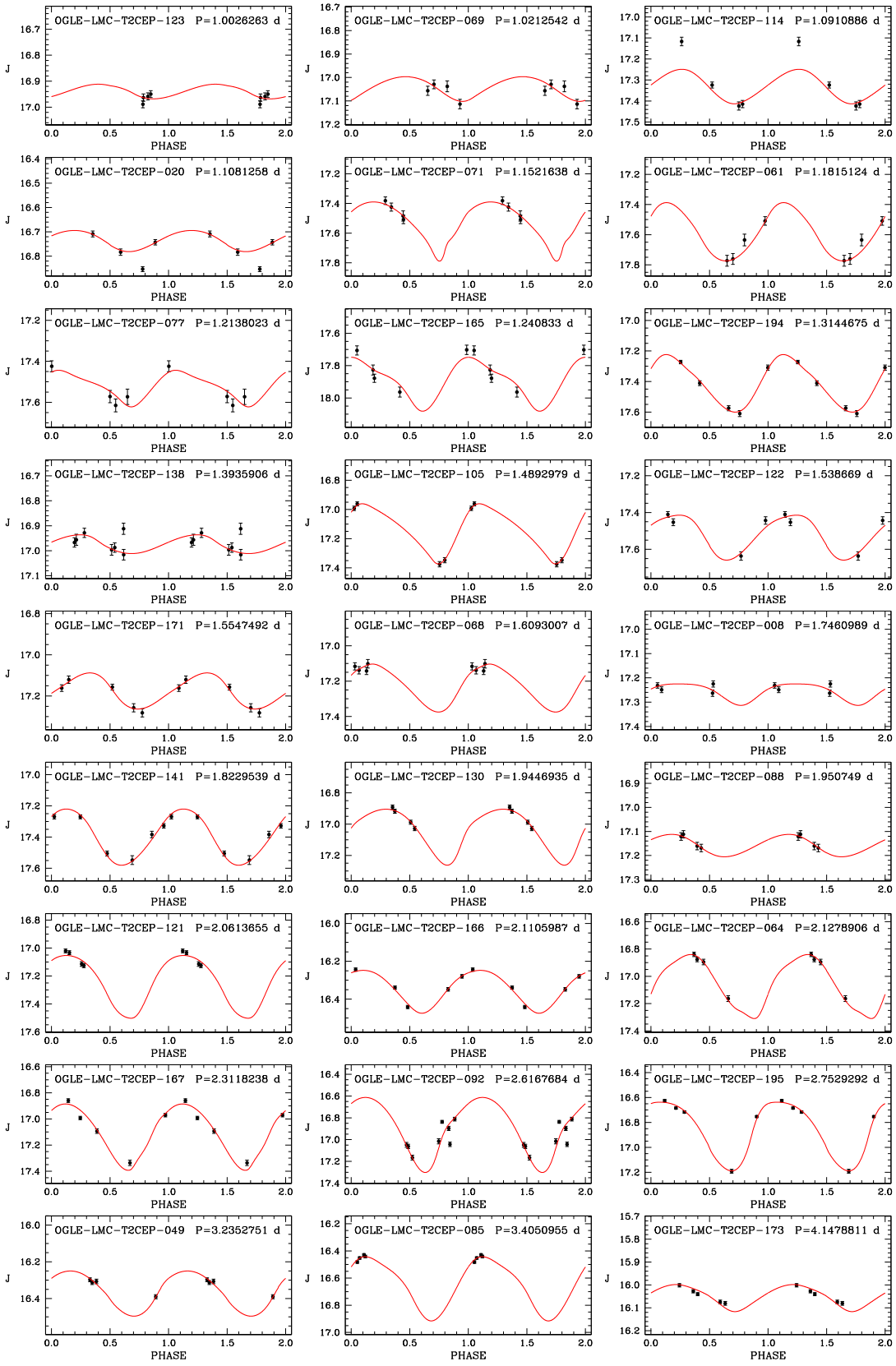

Figure A4. *J*-band light curves for T2CEP stars not possessing a sufficient number of epochs to perform the spline fit to the data and for which template fitting was used (see the text). Stars are displayed in order of increasing period. Solid lines represent spline best fits to the data (see the text). In each panel, we report OGLE's identification number and period.

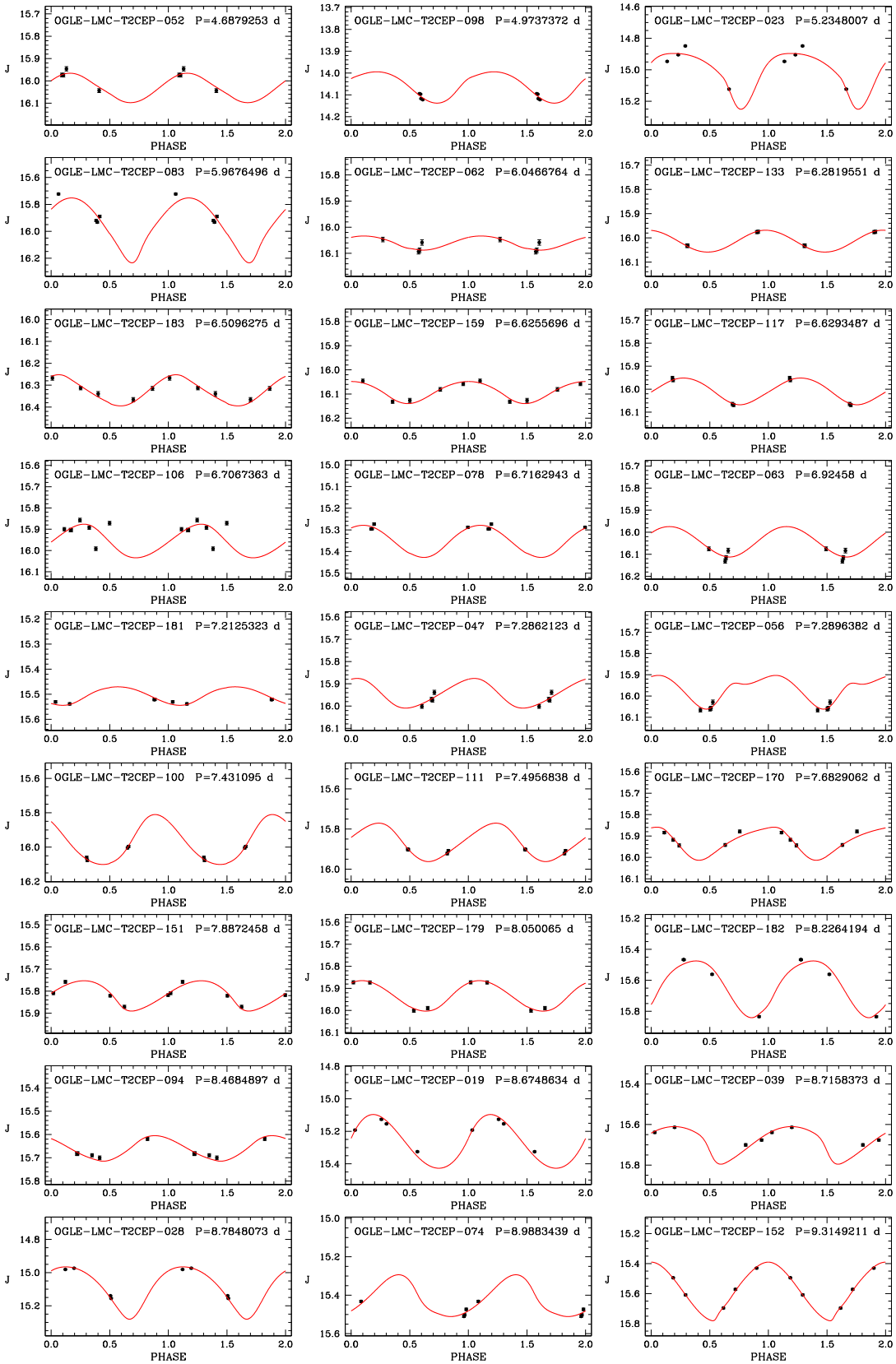

Figure A4 – *continued*

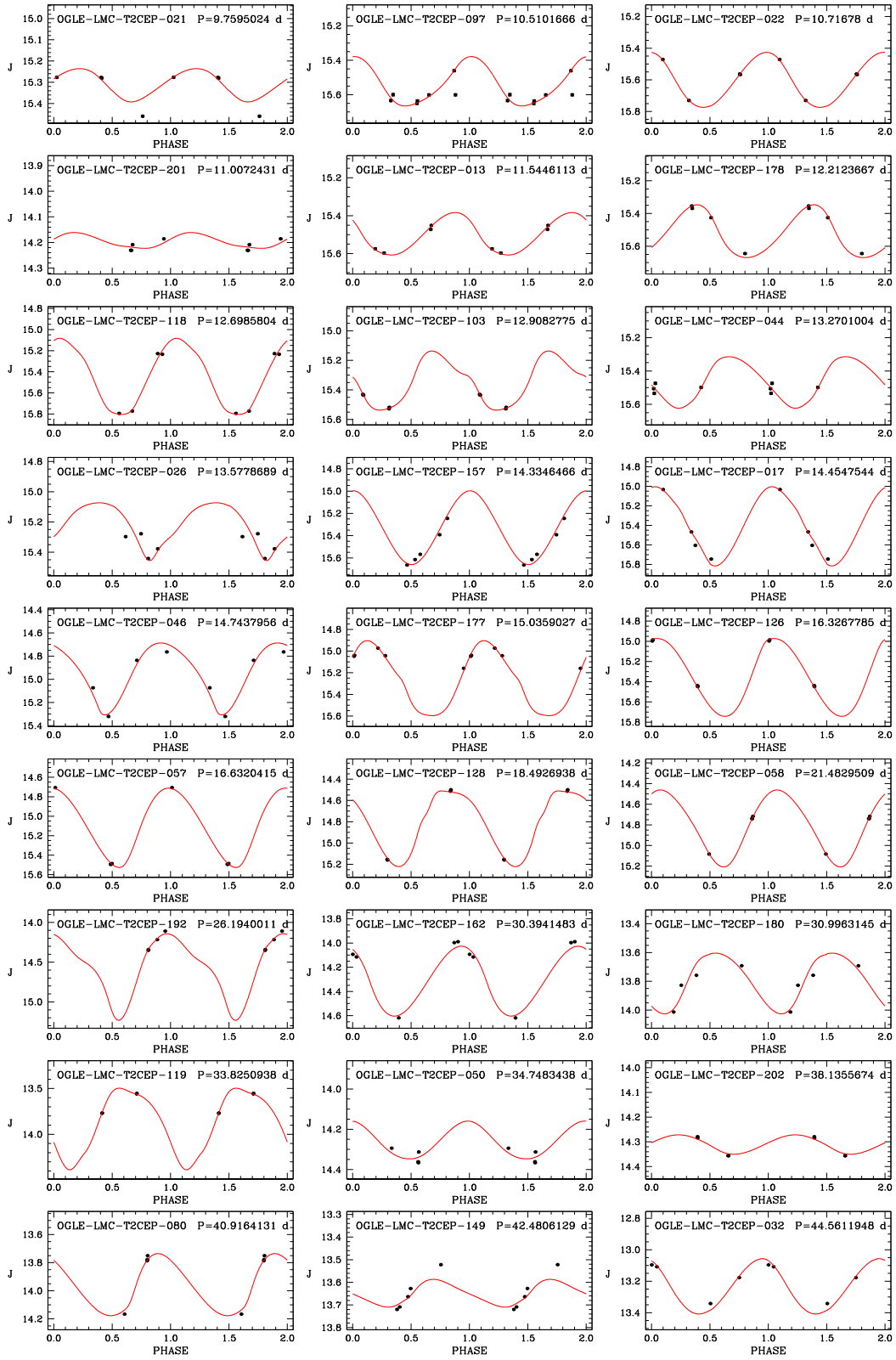

Figure A4 – *continued*

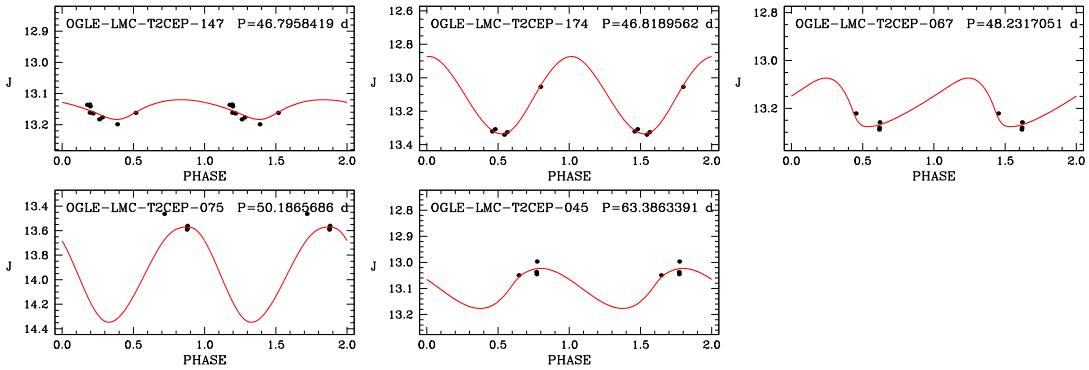

Figure A4 – *continued*

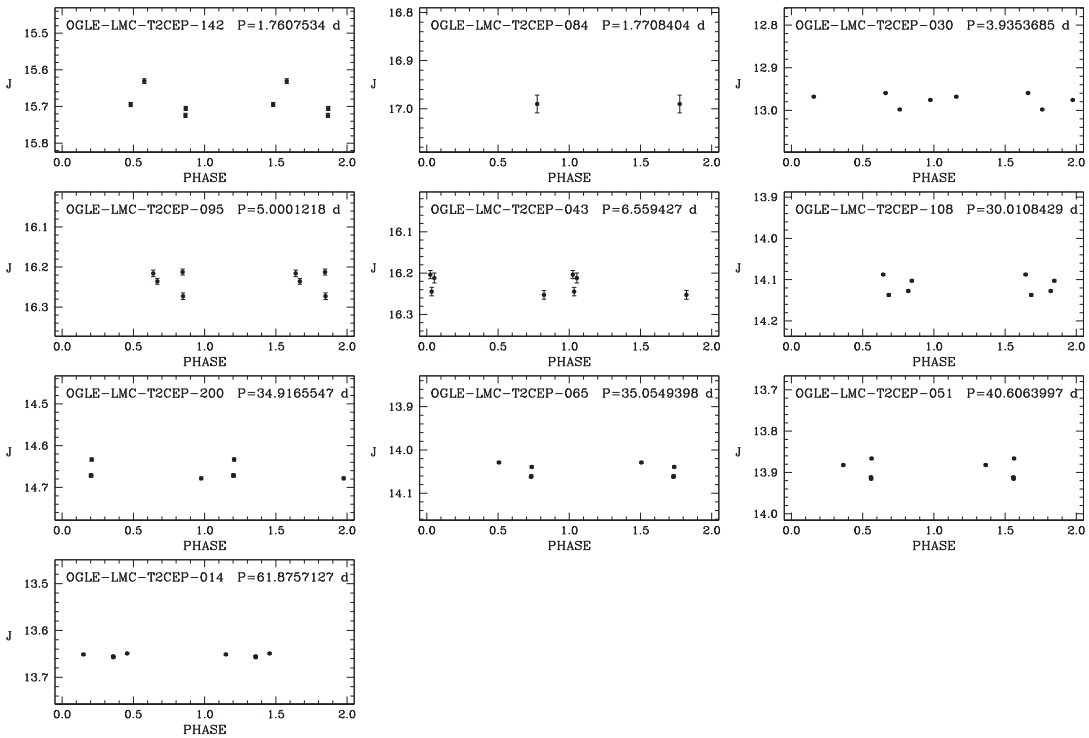

Figure A5. Light curves for stars showing problems in the J and K_s bands (see the text).

SUPPORTING INFORMATION

Additional Supporting Information may be found in the online version of this article:

Table 3. J and K_s time-series photometry for the T2CEPs investigated in this paper (http://mnras.oxfordjournals.org/lookup/suppl/doi:10.1093/mnras/stu2260/-/DC1).

Please note: Oxford University Press is not responsible for the content or functionality of any supporting materials supplied by the authors. Any queries (other than missing material) should be directed to the corresponding author for the article.

This paper has been typeset from a TEX/LATEX file prepared by the author.